CARRIER LIFETIME: FREE CARRIER ABSORPTION, PHOTOCONDUCTIVITY, AND PHOTOLUMINESCENCE

VYTAUTAS GRIVICKAS[1] AND JAN LINNROS[2]

[1]Institute of Applied Research, Vilnius University, Vilnius, Lithuania
[2]Royal Institute of Technology, Kista-Stockholm, Sweden

INTRODUCTION

The charge carrier lifetime is one of the most important parameters characterizing a semiconductor. This is mainly for two reasons: (1) the carrier lifetime determines the performance of devices while, at the same time, (2) it is a sensitive measure of material quality and cleanliness. Carrier lifetime may impact device operation directly, such as by affecting the turn-off speed of a diode or a thyristor operating at high injections, the leakage current of a *p*–*n* junction, or the excess carrier collection efficiency of a solar cell. Carrier lifetime may also affect operation indirectly, for example, by affecting the current gain and residual voltage drops of a bipolar transistor. Thus, a high carrier lifetime is desirable in many cases, whereas a low lifetime favors specific applications, for example, high-speed operation by shortening of switch-on or switch-off times as well as for generation of short terahertz pulses. Furthermore, for optically active devices, one is mainly interested in radiative recombination, and other recombination mechanisms must be suppressed to enhance quantum efficiency.

To monitor material quality and cleanliness, for example, during cleanroom processing, the carrier lifetime is one of the most sensitive parameters available being able to detect impurities down to a level of $\sim 10^{10}\,\mathrm{cm}^{-3}$ (Schroder, 1997), that is, one impurity atom per $\sim 10^{12}$ host atoms! In fact, for silicon, the highest lifetimes ever reported, that is, ~40 ms, (Yablonovitch et al., 1986; Pang and Rohatgi, 1991) are still believed to be limited by impurity/defect recombination and not by intrinsic recombination mechanisms such as radiative recombination. This makes lifetime characterization an important tool for verifying material quality and also for monitoring contamination during subsequent processing. Thus, lifetime measurements are also performed during CMOS processing even though field-effect transistors are unipolar devices, and thus not directly affected by the carrier lifetime (except for leakage current).

Carrier lifetimes and lifetime-characterization techniques have been studied extensively since the start of semiconductor research. This has resulted in the development of a large number of techniques based on different physical principles (Orton and Blood, 1990; Schroder, 1990). Yet, very few standard techniques exist and no single technique is dominant. This is in part due to the different requirements for various semiconductor materials, reflecting vastly different lifetime values, but also due to different geometry and probing depths.

Characterization of Materials, edited by Elton N. Kaufmann.
Copyright © 2012 John Wiley & Sons, Inc.

Finally, different recombination mechanisms or injection ranges are addressed by the different methods as they focus on various applications of the material or the device. As a consequence, different lifetime measurement techniques often yield vastly different results, even for the same sample!

This article briefly reviews the theory and common concepts in carrier-lifetime measurement methodology and focuses on a few important and general techniques used to characterize lifetime in semiconductor materials. Thus, device lifetime characterization methods have been left out. We do not intend to provide detailed descriptions of the reviewed methods; this information can be gathered from the cited references. Our aim is instead to present basic principles of the methods, methodology, and associated difficulties, such that the reader will be able to critically analyze data provided by the methods and to perform simple measurements using the techniques. Also, a selection guide is provided to direct users to the most appropriate method for their specific needs.

The three basic methods described in this article are free-carrier-absorption (FCA), photoconductivity (PC), and photoluminescence (PL). We have selected these methods based on the following criteria.

Free Carrier Absorption (FCA) is a pump–probe method which is fairly widespread and is a very general tool applicable to most semiconductor materials and also to some device structures and nanostructures. It provides an exceptional advantage, as different geometries and very different injection regimes can be realized, and therefore many different materials and recombination mechanisms may be characterized. We use it here to illustrate common concepts in FCA-based lifetime measurement methods, and, as a consequence, it is presented first. An alternative method, the so-called Transient grating method will be also briefly explained.

Photoconductivity (PC) is a standard method widely used for wafer fabrication quality monitoring and for clean-room process monitoring. It can be arranged in a number of different ways (by dynamic, light-modulated, and quasi-steady-state regime) using optical excitation. The carrier transients are detected by electrical contacts or by using contactless probing of the conductivity.

Photoluminescence (PL) is a particularly useful method for characterizing direct-bandgap semiconductors (having high quantum yields for radiative recombination), but has also been applied to indirect bandgap materials. Nowadays, it has become the mostly applied method for lifetime measurements in various nanostructures. This relies on the extreme sensitivity of many photodetectors, whereby even single-photon counting is available in most optical laboratories. The PL method has also become the workhorse when small volumes must be analyzed, such as in thin-film studies, quantum-wells or individual quantum dots or quantum wires for the rapidly expanding field of semiconductor nanostructures.

The article commences with a short review (see Section "Theory, below) of the carrier lifetime concept and various recombination mechanisms, also illustrating some major difficulties affecting lifetime characterization, such as trapping and surface recombination. The next section briefly outlines the different techniques and their fundamental principles of operation. Next, the three different techniques are described in detail. Finally, a selection guide is provided for the different lifetime applications.

THEORY

Carrier Lifetime Concept

In a semiconductor at equilibrium at a certain temperature, a balance exists between thermal generation of carriers, that is, electron–hole pairs, and recombination of carriers, such that the electron and hole concentrations, designated by n and p, respectively, remain constant (for a general textbook see Sze, 1981). In this way, the law of mass action, $np = n_i^2$, is fulfilled, where n_i is the intrinsic carrier concentration at this temperature. For any departures of the carrier concentrations from this balance such that the mass action law is no longer valid, the system will try to revert to equilibrium. In a general case, this is governed by the continuity equation

$$\frac{dn}{dt} = \frac{1}{q}\frac{\partial J_n}{\partial x} + (G_n - R_n) \tag{1}$$

where q is the elementary charge, J_n the electron current density, and G_n and R_n the generation and recombination rates for electrons in the semiconductor, respectively. A similar equation holds for holes. Assuming that no electric field is present, the current density is given only by a diffusion current

$$\frac{dn}{dt} = D_n\frac{\partial^2 n}{\partial x^2} + (G_n - R_n) \tag{2}$$

which is known as the diffusion equation, where D_n is the electron diffusion coefficient, which has been assumed independent of concentration and position. In a *homogeneous* case, the derivative with respect to x vanishes and a very simple equation remains. However, to treat the generation and recombination terms more easily, one may expand carrier densities in terms of excess concentrations Δn and Δp

$$n = n_0 + \Delta n;\ p = p_0 + \Delta p \tag{3}$$

Also, one may note that band-to-band recombination must be proportional to the product of n and p: that is, $R_n = Bnp$, where B is the radiative recombination coefficient. In thermal equilibrium, this recombination must be balanced by the band-to-band generation rate; thus, $G_n = Bn_0P_0$. Inserting into Equation 2, and for the homogeneous case one arrives at

$$\frac{d\Delta n}{dt} = -B(n_0\Delta p + p_0\Delta n + \Delta n\Delta p) \tag{4}$$

From this expression, it is clear that the system will revert to equilibrium both from a case where *excess carriers* have been introduced (i.e., when Δn and Δp are positive) as well as for a case where a *carrier deficit* is present (when Δn and Δp are negative). Examples of these situations are the return to equilibrium, (a) following an optical generation pulse and, (b) following a reverse biasing pulse forming a depletion layer as in a deep level transient spectroscopy (DLTS) experiment (deep level transient spectroscopy).

Examination of Equation 4 further reveals that two cases may be distinguished: (1) When Δn and Δp are small with respect to their equilibrium values (n_0,p_0) and (2) when they are much larger than they are at equilibrium. The former case is called low-level injection (ll) case, which is sometimes called *minority carrier injection*, while the latter case is referred to as the *high-level injection* (hl) case. We see that recombination is linear in Δn for the ll case and quadratic in Δn for the hl case for band-to-band recombination. As a final simplification, we will consider the case when Δn equals Δp, as in optical generation of carriers or during forward injection in a p–n junction diode (in a case of negligible trapping; see Section "Trapping" below). For minority carrier injection, Equation 4 reduces to

$$\frac{d\Delta n}{dt} = -B(n_0 + p_0)\Delta n \tag{5}$$

The solution to this equation is a simple exponential decay

$$\Delta n(t) = \Delta n(0) \cdot \exp(-t/\tau) \tag{6}$$

with lifetime $\tau = 1/[B(n_0 + p_0)]$ as given by Equation 5. The exponential decay and the lifetime defined in this manner are analogous to the decay of radioactive isotopes. More generally, the lifetime may be defined using a general recombination term R according to

$$\tau(t) = -\Delta n/R = -\frac{\partial}{\partial t}\ln[\Delta n(t)] \tag{7}$$

where R is the recombination rate of excess electron–hole pairs. The lifetime may not be a constant as in Equation 5, but may be a complicated function of injected carrier density, that is, of Δn and Δp, the position in the sample and of other carrier transport parameters.

Recombination Mechanisms

In the derivation of the rate equation governing recombination leading to Equation 5, radiative band-to-band recombination was assumed to be the single recombination mechanism, dominant in direct-bandgap semiconductors. However, several physically different recombination mechanisms can act simultaneously each of them adding a recombination term to Equation 2. Indeed, all of these mechanisms also have their corresponding generation mechanism, as stated in the *principle of detailed balance* (Van Roosbroeck and Shockly, 1954). Thus, a generation term must be added for each of them. This ensures that dn/dt equals zero at equilibrium, such that the carrier concentrations are maintained at the n_0 and p_0 values. Note that all equations should be valid both for intrinsic material as well as for doped or heavily compensated semiconductors.

In Figure 1, a few common recombination mechanisms are depicted. The first one, the SRH (Hall, 1952; Shockley and Reed, 1952) dominates recombination in most indirect bandgap semiconductors, such as Si, and involves the trapping of an electron at a recombination defect level within the bandgap followed by the capture of a hole to the same state (and at the same physical location). The reaction may start with the hole capture, depending on the relative capture strengths for holes and electrons and their relative concentrations, but effectively results in the loss of one pair of carriers upon completion. Since recombination is directly proportional to the trap concentration, the corresponding lifetime is a measure of the defect concentration in the sample. The lifetime may be calculated (Sze, 1981) from the effective SRH recombination rate (actually G–R in Equation 2)

$$R_{SRH} = \frac{pn - n_i^2}{\tau_p\{n + n_i \exp[(E_T - E_i)/kT]\} + \tau_n\{p + n_i \exp[(E_i - E_T)/kT]\}} \tag{8}$$

where E_T and E_i are the trap energy level and the Fermi energy level for intrinsic material, respectively, T is the absolute temperature, and k is the Boltzmann constant. τ_p and τ_n are defined as

$$\tau_p = \frac{1}{\sigma_p v_{\text{th}} N_T}; \qquad \tau_n = \frac{1}{\sigma_n v_{\text{th}} N_T} \tag{9}$$

where v_{th}, N_T, σ_p, and σ_n denote thermal velocity, available trap density, and cross-sections for hole and electron capture by the trap, respectively. The SRH lifetime

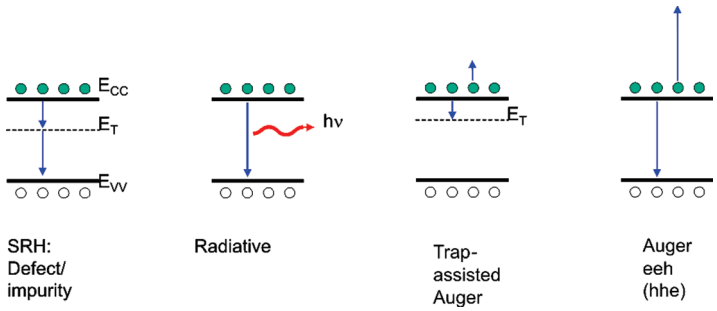

Figure 1. Typical recombination mechanisms in semiconductors. From left to right: (**a**) recombination through deep traps (SRH); (**b**) radiative recombination; (**c**) trap-assisted Auger recombination; (**d**) band–band Auger recombination. Reprinted with permission from Linnros (1998a). Copyright 1998, American Institute of Physics.

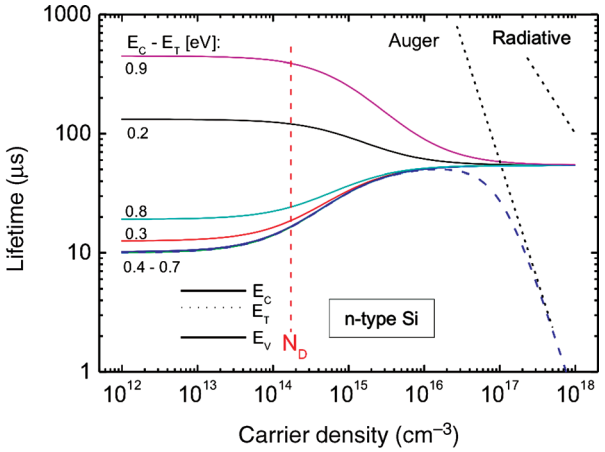

Figure 2. The lifetime injection dependence in n-type Si, doped to $10^{15}\,cm^{-3}$, for recombination through traps according to the SRH formalism (solid curves) with trap energy level as parameter ($\tau_p = 10\,\mu s$, $\tau_n = 44\,\mu s$). The radiative and Auger recombination rates are shown as dashed lines using generally accepted values for their respective cross sections. The long-dash line includes SRH ($E_c - E_T = 0.5\,eV$) and Auger recombination. Reprinted with permission from Linnros (1998a). Copyright 1998, American Institute of Physics.

may be derived using Equations 3 and 7 assuming $\Delta n = \Delta p$, and is given by the expression

$$\tau_{SRH} = \frac{\tau_p(\Delta n + n_0 + n_i e^{(E_T - E_i)/kT}) + \tau_n(\Delta n + p_0 + n_i e^{(E_i - E_T)/kT})}{p_0 + n_0 + \Delta n} \tag{10}$$

Figure 2 displays the functional form of τ_{SRH} versus carrier injection level, and with energy level, relative to the edge of the conduction band ($E_C - E_T$). In this example, *n*-type Si with a doping concentration of 1×10^{15} cm^{-3} was selected, and lifetime values were fixed to $\tau_p = 10\,\mu s$ and $\tau_n = 44\,\mu s$, respectively. From the figure, it is clear that trap energy levels close to the middle of the band gap are most efficient under minority carrier injection, while at high injections all levels are equally effective. The high-injection lifetime, from Equation 10 for infinite Δn, is given by

$$\tau_{hl} = \tau_n + \tau_p \tag{11}$$

The second recombination mechanism depicted in Figure 1 is the *radiative* process, or band-to-band recombination, where an electron and a hole recombine, resulting in the emission of a photon with the characteristic energy of the band gap. From Equation 4, ($\Delta n = \Delta p$) the radiative lifetime is given by

$$\tau_{RAD} = [B(n_0 + p_0 + \Delta n)]^{-1} \tag{12}$$

which is valid also at high carrier injection. While the intrinsic radiative lifetime dominates recombination in direct-bandgap semiconductors, B is about four orders of magnitude smaller in indirect semiconductors such as Si and Ge (see Section "Photoluminescence", below, and Table 1).

The third recombination process depicted in Figure 1 is *trap-assisted Auger* recombination (Landsberg, 1987). Here, the capture of an electron (or a hole) at a trap is not accompanied by phonon emission as in the usual SRH case, but its energy is instead transferred to a second electron (or hole). The rate equation in this case predicts a quadratic dependence in carrier concentrations (i.e., proportional to *np*, *nn*, or *pp*) just as in the case of radiative recombination; however, the rate constant is also proportional to the trap density. Therefore, radiative and trap-assisted Auger may be combined into a common radiative coefficient according to

$$B = B_{RAD} + \beta_{TRAP} \cdot N_T \tag{13}$$

where B_{rad} signifies the purely radiative coefficient and β_{trap} is a coefficient for the trap-assisted process.

Finally, *Auger recombination*, depicted as the fourth mechanism in Figure 1, is the recombination of an electron and a hole while the energy is transferred to a third carrier. As three carriers are involved, Auger recombination only dominates at very high injections. However, in highly doped semiconductors, as in emitter regions of devices, Auger recombination becomes large and often sets the lifetime in these regions. At high injections, the Auger lifetime is given by

$$\tau_{Aug} = \frac{1}{(C_p + C_n) \cdot \Delta n^2} = \frac{1}{\gamma \cdot \Delta n^2}; \gamma \equiv C_p + C_n \tag{14}$$

where C_p and C_n are the Auger coefficients for the *hhe* and the *eeh* processes, respectively. In the minority carrier regime, the Auger lifetime is defined as

$$\tau_{Auger} = \frac{1}{C_p p_0^2}; \quad \tau_{Auger} = \frac{1}{C_n n_0^2} \tag{15}$$

representing the Auger lifetime in highly doped *p*-type and *n*-type material, respectively. Note that both C and γ are used to denote Auger coefficients and B and β are used for the radiative coefficient.

For calculating the resulting total lifetime, one may note that according to Equation 2, recombination is additive, and when using Equation 7, lifetimes should be summed as inverse numbers

$$\frac{1}{\tau} = \frac{1}{\tau_{SRH}} + \frac{1}{\tau_{RAD}} + \frac{1}{\tau_{Auger}} \tag{16}$$

In Figure 2 the resulting total lifetime injection dependence is shown as a dashed line where Auger and radiative recombination in Si have been included with traditional values for B, C_p, and C_n (Schlangenotto et al., 1974; Dziewior and Schmid, 1977). The individual contributions of these recombination rates are shown as dotted lines. For the minority carrier *doping dependence* in Si, see, for example, Häcker and Hangleiter (1994) and Rohatgi et al. (1993). Finally, Table 1 reports typically measured carrier lifetimes for a few indirect-bandgap semiconductors and for GaAs.

Table 1. Measured Carrier Lifetimes and Typical Recombination Coefficients in Some Selected Semiconductors at 300 K[a]

Material	Measured Lifetimes	Radiative Coefficient (cm^3s^{-1})	Auger Coefficients (C_n) (cm^6s^{-1})	Auger Coefficients C_p (cm^6s^{-1})	$C_n + C_p$ (hl) (cm^6s^{-1})
Indirect					
Si	Typical: 10 to 200 μs Highest: 40 ms[e] Lowest: ~1 ps[f]	1×10^{-14}[b]	2.8×10^{-31}[c]	1×10^{-31}[c]	1.35×10^{-30}[d]
Ge	Typical: 1 to 200 μs	5.2×10^{-14}[g]	8×10^{-32}[g]	2.8×10^{-31}[g]	1.1×0^{-31}[h]
4H-SiC	Typical: 100 ns to 1 μs Highest: 20 μs[k]	1.5×10^{-12}[j]	5×10^{-31}[j]	2×10^{-31}[k]	7×10^{-31}[j]
3C-SiC	Highest: 150 ns	–	–	–	2.5×10^{-32}[k]
GaP	Highest: 10 ns	10^{-13}[k]	10^{-30}[k]	–	10^{-30}[k]
Diamond	Typical: 3–5 ns[l]	–	–	–	–
Direct					
GaAs	Typical: 1 ns to 2 μs[n]	2×10^{-10}[g]	1.8×10^{-31}[g]	4×10^{-30}[g]	7×10^{-30}[m]
GaN	Typical: 5–30 ns	2×10^{-11}[k]	–	–	–

[a]The resulting effective lifetime can be obtained using Equations 12–16, noting the appropriate injection level, Δn, in a particular measurement. The "apparent measured lifetime" is determined by impurity/defect recombination (SRH) except for clean material of direct-bandgap-type semiconductors where the lifetime is set by the radiative lifetime. The last column refers to measurements at high-level injection.
[b]Schlangenotto et al. (1974).
[c]Dziewior and Schmid (1977), on highly doped material.
[d]Refers to high-injection Auger coefficient in lowly doped material (Grivickas and Willander, 1999).
[e]Yablonovitch et al. (1986).
[f]Amorphous material (Smith et al., 1981).
[g]Schroder (1997, p. 362).
[h]Auston et al. (1975).
[i]Bergman et al. (1997).
[j]Galeckas et al. (1997a).
[k]*http://www.ioffe.rssi.ru/SVA/NSM/Semicond/*
[l]*CVD grown diamonds*, T. Malinauskas et al. (2010)
[m]Strauss et al. (1993).
[n]Wight (1990).

Radiative and Auger coefficients have also been included in the table. Coefficients for radiative and Auger recombination for other semiconductors may be found in Schroder (1990).

Trapping

In the treatment of recombination so far, it has been assumed that $\Delta n = \Delta p$ and that a single defect center is active with a single trap energy level. If, however, the defect concentration, N_T, is high relative to the doping density and injected carrier densities, Δn and Δp, recombination rates may be different for electrons and holes [due to their different capture cross-sections, $\sigma_{n(p)}$]. This leads to unbalanced carrier densities, resulting in non-exponential carrier decays (Macdonald and Cuevas, 2003; Warta, 2006; Klein et al. 2011).

A similar situation occurs when a high concentration of a shallow defect level is present in addition to the main recombination level. According to the most general definition (in Ryvkin, 1964, and in other textbooks) any level in the forbidden gap acts as a recombination level if its position is between the quasi-Fermi levels for electrons and holes. On the contrary, levels that are outside this region (i.e., outside quasi-Fermi levels at the particular injection) act as temporary traps. Traps may often be evidenced experimentally in compound compensated wide-bang gap semiconductors like GaN and SiC (Klein et al. 2011. A slow trapping decay due to minority hole capture on the n+ 4H–SiC substrate side is evidenced in (Klein et al., 2011). The carrier trapping is frequently observed in high energy particle irradiated materials and almost in all disordered amorphous semiconductors. In specific cases, a large density of trap centers exists, sometimes of different energy levels, E_T, which in most experiments exceeds the injected carrier density by several orders. A large capture cross-section for minority carrier and a small one for majority carrier temporarily holds the minority carrier before releasing it to the band again (the difference with a deep center being that emission to the band of an electron is far more probable than completion of the recombination by the capture of a hole). This results in variable time delay before recombination through the main recombination level takes place, yielding a slow, transient component. For a single minority carrier captured by the trap, the temperature variation of the slow component can provide values for the main trap parameters (Ichimura, 2006; Klein et al. 2011. However, the necessary analysis is not simple because four typical cases, both for capture and detrapping, (multiple trapping) should be taken into account.

Generation (Detrapping) Lifetime

When a carrier deficit exists, that is, when both Δn and Δp are negative, recombination according to Equation 8 is negative, meaning that carriers are generated. This

carrier generation is mediated through the trap level acting as a stepping stone to cross the band gap and is much more efficient than ordinary band-to-band generation. Such a situation exists, for example, in the depletion layer in a device, and carrier generation results in additional leakage currents. As a consequence, recombinative defects are also important for majority carrier (unipolar) devices such as MOS transistors.

The generation lifetime may be derived from the SRH expression, Equation 8, in the limit when pn reduces to zero (also $n = p = 0$) and is given by

$$\tau_g = \tau_p \exp[(E_T - E_i)/kT] + \tau_n \exp[(E_i - E_T)/kT] \qquad (17)$$

Analyzing Equation 17, one finds that for $E_T \cong E_i$ the generation lifetime is of the same magnitude as τ_n and τ_p. However, for trap levels far from the intrinsic Fermi level, E_i, the generation lifetime may be orders of magnitude larger than the corresponding recombination lifetime. Thus, we conclude that lifetime measurement techniques probing the generation lifetime, for example, the *pulsed MOS capacitance* technique, should not be used to measure the recombination lifetime, which is important for bipolar devices as in the base of a transistor, for example. This was extensively discussed by Schroder (1990) and Baliga (1987).

Aspects of Surface Recombination and Diffusion

Inspection of Equation 2 reveals that the local excess carrier decay is not only affected by recombination, which is of primary interest here, but is also affected by carrier gradients. Carrier gradients may result not only from an inhomogeneous excess carrier excitation, but also from differences in the local recombination rate. The effect may be dramatic, such that the diffusion term (all three coordinate directions need to be considered) totally dominates dn/dt and no useful information can be extracted for the recombination term. In fact, diffusion is a limiting factor for most lifetime measurement techniques, and, for an initially homogeneous excess carrier profile, local lifetime information is only obtained within a radius of a *diffusion length*, L_D, given by

$$L_D = \sqrt{D \cdot \tau} \qquad (18)$$

For low carrier lifetimes, as occurs in direct-bandgap semiconductors, the diffusion length is relatively short and the spatial resolution is usually set by the specific lifetime measurement technique. In contrast, in indirect-gap semiconductors of good quality material, characterized by high carrier lifetimes, the diffusion length may be several hundred microns. In this case, carriers easily reach sample or wafer surfaces and the state of these surfaces becomes critical. Thus, high surface recombination results in a flow of carriers toward the surfaces, leading to a drainage of carriers in the interior bulk and an incorrectly determined value for the carrier lifetime. This is illustrated in the leftmost schematic of Figure 3 and confirmed by the experimental data of Figure 4a in surface excited passivated silicon and Figure 4b in bulk-like excited 45 μm thick 4H–SiC epilayer grown on a heavily doped n^+ substrate. In the last case, instant carrier density profiles are shown as measured following a short optical generation pulse. The data clearly illustrate the effect of surface recombination, which dominates the observed lifetime. Notably, surface recombination is not a different recombination mechanism, but simply SRH recombination occurring at the surface, for example, at dangling bonds. By the same token, defects *close* to the surface may not be distinguished from defects at the surface.

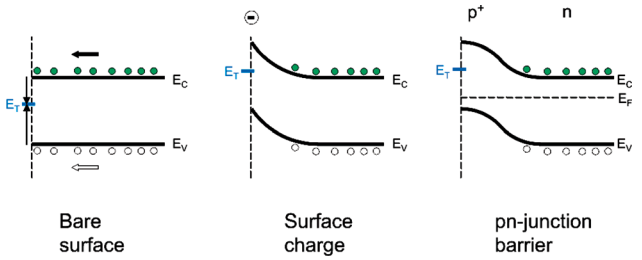

Figure 3. Influence of surface on carrier dynamics. From left to right, schematics illustrate (**a**) high surface recombination at a bare, nonpassivated surface; (**b**) shielding of surface states due to charge-induced band bending; and, finally, (**c**) barriers introduced by a p–n junction (also shielding the surface).

Surface recombination is described by the surface recombination velocity, s, in units of cm/s. Its defining equation is

$$D(dn/dx) = -s \times n \qquad (19)$$

In the case of the 4H–SiC interface, the carrier leakage through the barrier occurs due to doping-related difference of the bandgap between the epilayer and the n^+ substrate. In the high injection limit, this leakage can be treated with a boundary condition with an effective surface recombination which depends on substrate doping. The air–semiconductor surface recombination velocity depends on various surface treatments and can be as high as 10^6 cm/s for a mechanically polished surface. The solutions of the diffusion equation, Equation 2, in a one-dimensional transient case, with boundary values for the surface recombination velocity according to Equation 19, are nonanalytic (Waldmeyer, 1988). For long times after the initial excitation, however, a "steady-state" carrier profile develops, resulting in an exponential excess carrier decay. The corresponding effective lifetime, τ, is modified by the "surface lifetime," τ_s, according to

$$\frac{1}{\tau} = \frac{1}{\tau_b} + \frac{1}{\tau_s} \approx \frac{1}{\tau_b} + \frac{1}{d\left(\frac{1}{2s} + \frac{d}{D\pi^2}\right)} \qquad (20)$$

where τ_b is the bulk lifetime, D the diffusivity at the appropriate injection, and d the smallest dimension of the sample (usually the wafer thickness). The last approximate equality holds for the specific case where the two surfaces are identical, that is, $s_1 = s_2 = s$. This approximation was proposed by Grivickas et al. (1989),

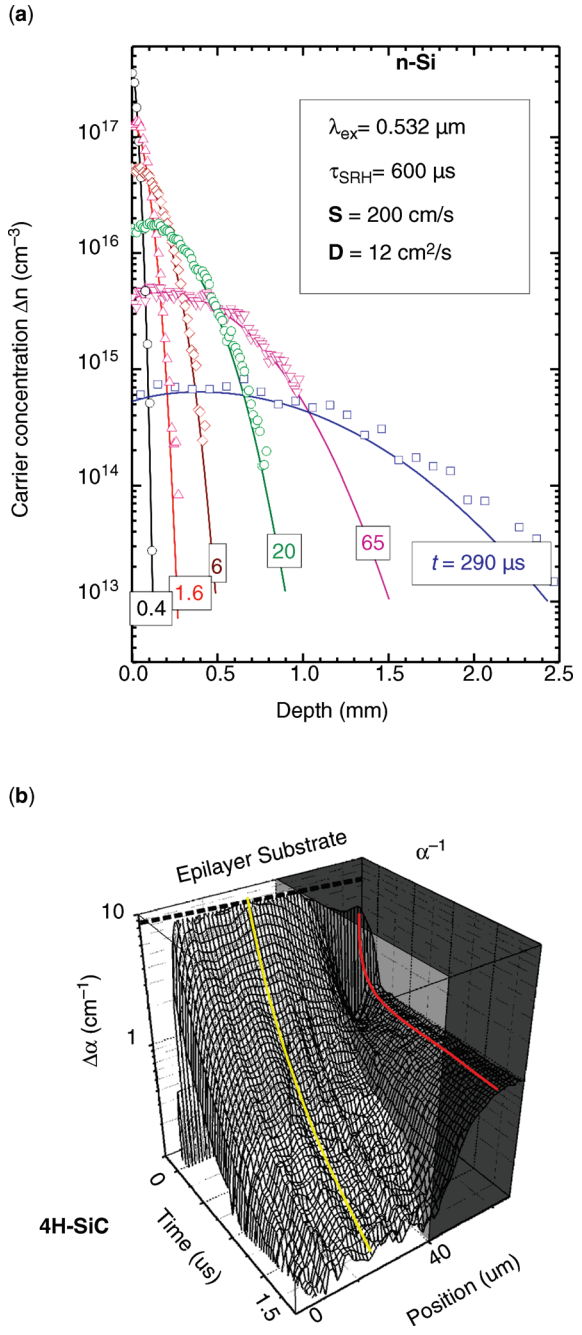

Figure 4. (**a**) Depth-resolved free-carrier-absorption dynamics in n-Si sample ($10^{15}\,cm^{-3}$) following a pulsed 90 ns photoinjection from the oxygen passivated (left side) surface. Modeling parameters are used for theoretical represents calculations (curves) of carrier diffusion profiles at successive time moments. After Grivickas et al. (2000). (**b**) Similar dymamics obtained in n-4H–SiC epilayer-(p+)substrate structure. The top surface (left side) is covered by oxide while the interface is located at 45 μm depth position. The peak value of the photoinduced absorption in the epilayer corresponds to $5 \times 10^{17}\,cm^{-3}$ injected carrier concentration. Absorption slope, α^{-1} is indicated by dashed line. Lifetime time dependence in mid of epilayer and in the substrate is exaggerated by two thick lines. Reprinted from Grivickas et al. (2000), Copyright 2000, with permission from Elsevier.

the uncertainty being less than 4% over the entire range of s values. Note that, for a single active surface the factor of two in the denominator of Equation 20 should be removed, Sproul (1994).

Figure 5a shows the results of a calculation according to Equation 20 of the effective lifetime in a Si wafer as a function of thickness. Data for two values of the surface recombination velocity are displayed, and in the calculation an ambipolar diffusivity of $D_a = 17\,cm^2/s$ was used (Linnros and Grivickas, 1994). The data illustrate well the limitation in measured lifetime imposed by surface recombination, which may only be solved using well-passivated sample surfaces or extremely thick samples ($d^2 \gg D\pi\tau_b$). Figure 5b shows the effective lifetime measured in a 4H–SiC epilayer of different thicknesses. The shaded area designates the range of experimentally verified surface recombination velocities obtained by a proper lifetime modeling (almost the same as according to Equation 20; Galeckas et al. 2001).

Methods to reduce high surface-recombination rates are nontrivial, and, in general, such methods may alter the lifetime distribution or may involve etching of the surface. For silicon and some other semiconductors, a thermal oxide of good quality or surface nitridation may reduce surface recombination substantially, although the high-formation temperature would probably alter the defect distribution of the sample. Other methods involve different surface passivation schemes, or even measurements with the Si wafer immersed in a passivating HF bath (Yablonovitch et al., 1986). A different approach involves the creation of charges at the surface, resulting in a surface band bending, as illustrated in the middle panel of Figure 3 (Katayama et al., 1991). Finally, the right part of Figure 3 shows the situation when a p–n junction is present, as in a highly doped emitter in a device. In this case, the bending of the bands results in barriers, which reflect either electrons or holes (being minority carriers in the highly doped region) such that recombination is inhibited (Linnros, 1998a). Thus, a measurement in the n region would reflect the "true" bulk lifetime.

Related Physical Quantities

Although the primary concern of this article is lifetime measurement techniques, several of these methods may be used to extract other related physical quantities. In fact, some methods do not even measure the lifetime directly, but extract the lifetime from the measurement of other quantities such as the diffusion length. A summary of related physical quantities and a brief comment on how they can be measured is displayed in Table 2.

OVERVIEW OF CARRIER LIFETIME CHARACTERIZATION TECHNIQUES

In this section, a brief overview of the most common methods for carrier lifetime characterization will be given. We do not intend to provide a full list of all methods; examples can be found in the textbook of

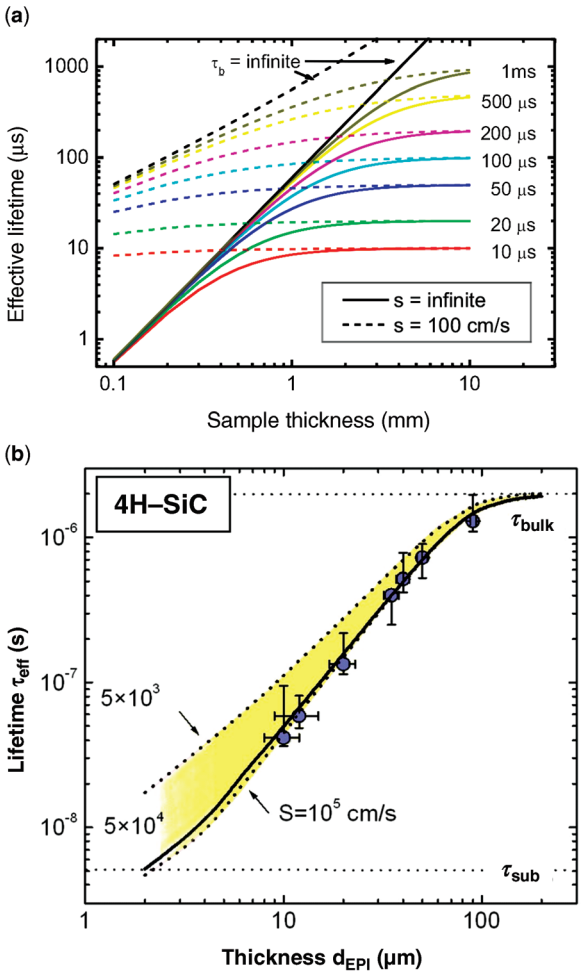

Figure 5. (**a**) Calculated effective lifetime in silicon, with bulk lifetime as a parameter, versus sample thickness. Solid lines—assuming infinite surface recombination an ambipolar diffusion coefficient D of 17 cm^2/s. The dotted curves were calculated using Equation 20 with a surface recombination velocity of 100 cm^2/s. (**b**) Effective carrier lifetime as a function of epilayer 4H–SiC thickness. Points represent experimaental data obtained by FCA. Curves are simulated numerically (D= 2.6 cm^2/s). Shaded area designates the range of experimentally verified surface recombination velocity. Typical lifetime in heavily doped substrate τ_{sub} is also indicated. Reprinted with permission from Galeckas et al. (2001). Copyright 2001, American Institute of Physics.

Schroder (1990) and that of Orton and Blood (1990), and by Klein (2008). Instead, we will focus on fundamental principles of operation, applicability, and strengths and weaknesses. Finally, a comparison of a few techniques from the viewpoint of certain criteria will be provided together with a selection guide.

For an overview, the different methods may be sorted in several different ways: either according to physical principles, according to methods used for carrier injection, according to methods used for probing of excess carriers, or according to whether techniques are contactless, nondestructive etc. Unfortunately, there are no unambiguous ways to perform such sorting, partly because variants of the same method would fall into different categories. The approach taken here is to divide the methods into *optical techniques*, *diffusion length-based methods*, and *device-related techniques*. We note that this distinction is not clear, as optical techniques may contain current probing (as in photoconductivity) and diffusion length-based methods normally use optical excitation for carrier injection. In addition, several variants exist of techniques where electrical injection is replaced by optical injection, or vice versa. Finally, all techniques may be classified into steady-state methods, modulated methods, or transient/pulsed methods. Several of the methods presented here, indeed, exist in two or all three of these variants.

Optical Techniques

Figure 6 shows the principles of three different techniques based on optical injection of excess carriers. The carriers, that is, electron–hole pairs, are normally generated by a laser or other light source with photon energy larger than the fundamental energy gap of the semiconductor. The impinging light beam may be continuous, modulated, or pulsed. The resulting excess carrier concentration is either maintained at a higher nonequilibrium value depending on lifetime (if the impinging light is continuous), mimics the imposed modulation with some possible delay (if the light is modulated), or exhibits a transient decay following the initial excitation pulse (if the light is pulsed).

In the PC method, excess carriers represent a modulation of sample conductivity, which is sensed as a current increase in the external circuit. Contactless variants of this method are the *microwave PC-decay* method and the *radio-frequency PC-decay* method. In the former method, excess carriers are probed by microwaves reflected due to a change in the dielectric constant of the sample resulting from the excess carriers. In the latter technique, excess carriers are detected by a coil reacting on the difference in sample conductivity (see Fig. 6).

The PL method is only applicable for semiconductors exhibiting radiative recombination. This is not a severe limitation, as PL techniques are extremely sensitive and may also be used for semiconductors of indirect bandgap. PL emission will occur from regions of the sample where the excess carrier density is highest. Filtering to a specific wavelength range is a main advantage, reducing background noise and allowing recombination studies of a particular material (e.g., in multiple layer structures). Note that the PL yield tracks the excess carrier density through the radiative process, even in the presence of other possibly dominant recombination mechanisms.

Finally, in the FCA method, excess carriers are sensed by an infrared (IR) beam (or a visible beam, provided that the photon energy is lower than the bandgap energy) transmitted through the sample. The absorption is more or less proportional to the excess carrier density, allowing a calibration of the injected carrier density. The two-beam method can support several different geometries, facilitating depth-resolved studies.

Table 2. Carrier Lifetime and Related Physical Quantities[a]

Physical Quantity	Symbol	Injection Case	Dominant Regime	Measurement Principle (Examples)
SRH lifetime	τ_{SRH} (ll)	ll	Indirect semiconductor	See techniques of this article
	τ_{SRH} (hl)	hl		
Radiative lifetime	τ_{SRH} (ll)	ll	Direct semiconductor	PL-transient
	τ_{RAD} (hl)	hl		PL-transient
Auger lifetime	τ_{Auger} (ll); γ_n γ_p	ll	High doping	Measure ll-lifetime
	τ_{Auger} (hl); γ	hl	High injection	Nonexponential transient e.g., EBIC/OBIC
Diffusion length	L_D	ll		
Diffusivity	D_nD_p	ll		Time-of-flight, Transient grating
	D_a (ambipolar)	hl		Transient grating
Mobility	$\mu_n\mu_p$ (majority)	ll		Conductivity/Hall
	$\mu_n\mu_p$ (minority)	ll		Haynes–Shockley time-of-arrival method
Surface recombination velocity	s_ns_p	ll, hl	–	See several techniques of this article

[a]Some of these quantities may be determined in lifetime-type experiments. The fourth column indicates for which type of material a recombination mechanism is dominating while the fifth column indicates suitable measurement methods.

Diffusion Length-Based Methods

According to Equation 18, the carrier lifetime is proportional to the carrier diffusion length squared. The diffusion coefficient is taken to be constant. This is a good approximation in the low-injection case and for homogeneously doped material where the value of D can be found from mobility-doping data using Einstein's relation, $D = kT\mu/e$. At higher injection levels, however, this is no longer true, as the diffusion coefficient may change substantially when the ambipolar injection regime is approached, and for even higher injection levels, a decrease has been observed due to bandgap shrinkage (for Si see Linnros and Grivickas, 1994). Thus, we conclude that the carrier lifetime may only be obtained safely from a measurement of the diffusion length in the minority carrier regime. Furthermore, we note that, due to the short radiative lifetimes of direct-bandgap semiconductors, diffusion lengths are extremely short, making diffusion length-based methods less attractive for these materials.

Figure 7 presents principal schemes of four popular methods to measure diffusion lengths. In the *optical beam-induced current* (OBIC) method or in the *electron beam-induced current* (EBIC) method, excess carriers are generated locally by a focused laser beam or electron beam, respectively. The carriers diffuse in all directions and the fraction collected by an adjacent p–n junction will be detected as a current increase, ΔI, in the outer circuit. By varying the distance of impingement of the generation beam from the p–n junction depletion edge, the diffusion length can be measured and the local lifetime extracted.

Using a different geometry, where the p–n junction is present at the backside of a sample, lifetime mapping may be performed. Here, the fraction of carriers that reach the p–n junction will be collected as illustrated by the block arrow in the center panel of Figure 7. This

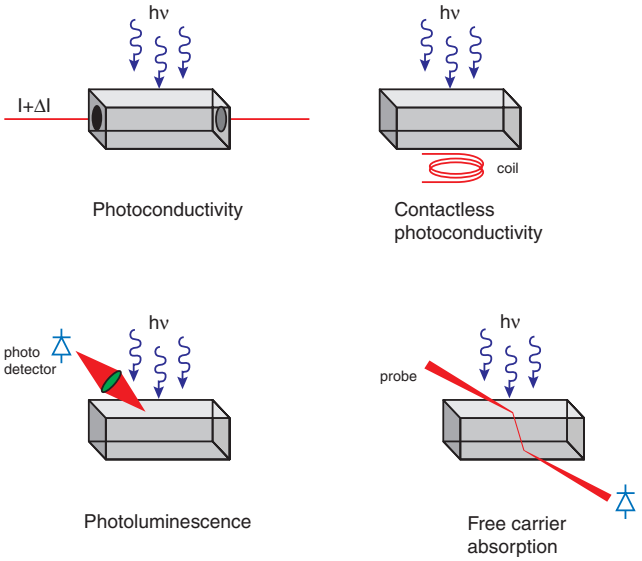

Figure 6. Principles of common optical techniques to measure carrier lifetime.

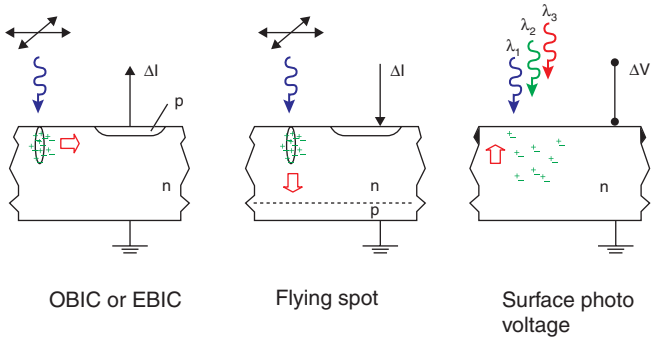

Figure 7. Principles of techniques to measure carrier diffusion lengths for lifetime derivation. Block arrows indicate direction of carrier flow toward p–n junction, or, for the surface photovoltage technique, toward the surface (shaded area indicating depletion zone due to band bending).

geometry may be used both in EBIC and OBIC experiments where, for the latter, it is sometimes called the *flying spot* technique (Bleichner et al., 1986). A main disadvantage of the technique is the sensitivity to surface recombination and charging effects on the surface (because in this case only a small fraction of the generated carriers are collected by the *p–n* junction).

Another technique which is suitable for lifetime mapping of bare wafers (without *p–n* junctions) is the *surface photo voltage* technique (SPV), see the right-hand panel of Figure 7. The surface of the probed sample is treated chemically to provide surface charges, inducing surface band bending. Excess carriers, generated optically, reach the surface to induce a voltage shift, ΔV, at the surface, which is measured by a local contact probe. The diffusion length can be extracted by measurements at different wavelengths to provide different penetration depths in the semiconductor (see Schroder, 1990).

Device-Related Techniques

Lifetime techniques based on device measurements fall into a separate class of methods, not because of different physical principles, but because they provide *local measurements* of the lifetime in operating devices (Galeckas et al., 2006, Giesecke et al., 2011). This is also a restriction, as for large component areas only an effective lifetime is obtained, averaged over device area and depth. The main advantage is the relatively simple setup, as measurements may be performed directly on the processed wafer, for example, at a probe station, facilitating automated measurements on a number of devices and with the help of only electrical instruments. In a few cases, measurements may also be performed without the detrimental effects of surface recombination, for passivated devices.

The left panel of Figure 8 shows a schematic of lifetime measurements performed on diode structures. In a first period of the measurement, electron–hole pairs are generated continuously during forward conduction by injection from emitters. Then, the circuit is broken by a fast electrical switch, resulting in an open circuit for the rest of the measurement interval, as in the *open circuit voltage decay* (OCVD) technique. If the lifetime of the excess carriers is significantly longer than the switching time, the carriers will remain within the device, their concentration decreasing as a result of recombination. For this time period, the diode will work as a solar cell, providing an open circuit voltage that decays logarithmically with carrier concentration. Thus, from the measured *V(t)* transient, the carrier lifetime can be deduced.

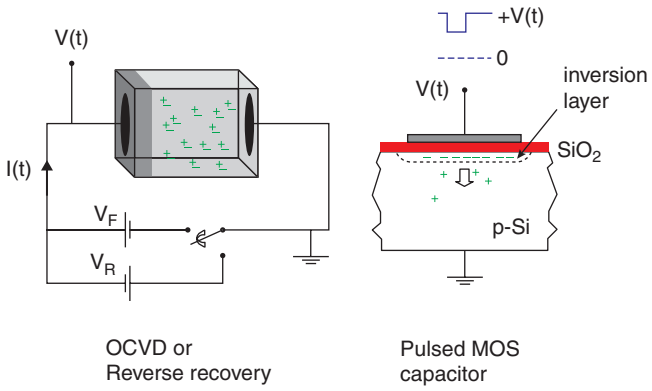

Figure 8. Principles of some device-related techniques.

In the alternative technique of *reverse recovery* (RR), the switch is not left open but is switched immediately to a reverse voltage. Under such conditions, the remaining excess carriers will support a large current in the reverse direction until carriers have been depleted at the *p–n* junction such that a depletion layer may form.

Finally, in the *pulsed MOS capacitor* technique, minority carriers are provided by an inversion layer, as in an MOS transistor channel. By subjecting the top electrode of the MOS diode to a voltage pulse, the minority carrier concentration in the inversion layer must change accordingly. However, this cannot happen instantaneously since, for a positive pulse (*p*-type Si), minority carriers must be generated thermally or, for a negative pulse, minority electrons must recombine. In the latter case electrons are pushed into the substrate to recombine with majority holes. Thus, for positive pulses, a transient measurement of the capacitance provides the generation lifetime, whereas a negative pulse yields the recombination lifetime. As described above (see Section "Theory"), these lifetimes generally have very different values. The main advantage of the method remains practical, as MOS diodes may be easily provided as test structures to obtain lifetime information on fully processed CMOS wafers.

STEADY-STATE, MODULATED, AND DYNAMIC METHODS

As stated in the beginning of this article, lifetime determination methods can be classified into three basic groups: quasi-steady-state methods, modulated methods, and dynamic (sometimes called pulsed or transient) methods (Ryvkin, 1964; Orton and Blood, 1990). In quasi-steady-state methods, a physical quantity, which is related to the excess carrier density concentration, is determined. Having additional knowledge about the carrier generation rate *G*, the effective carrier lifetime can be calculated *as* $\tau_{\text{eff}} = \Delta n/G$. A number of modulated methods for monitoring carrier lifetime depend on simultaneously monitoring the amplitude and the phase lag between a measured physical quantity and a sine- or square-wave-modulated light excitation. Dynamic methods depend on measuring the full change (decay process) of the measured physical quantity following an excitation pulse. These three regime concepts themselves cover many of the somewhat more specialized device-related techniques (e.g., carrier collection in depletion regions of *pn* junction devices) and also most of lifetime measurements based on diffusion length determination (Orton and Blood, 1990; Schroder, 1990). Here, a question naturally comes into mind as to whether there is any advantage or disadvantage to the measurement of lifetime by each of these method groups of methods.

The answer can follow two distinct paths. A simple answer is that in describing carrier lifetime we have to choose a preferable technique suited for a particular material, an expected range of lifetimes, and an expected accuracy of the measurement. For instance, one might prefer to use the modulated PL technique for characterizing light-emitting, highly doped, direct-bandgap semiconductors where the radiation yield is high and a lifetime is expected in 10^{-7} to 10^{-9} s range. It can be imagined that any dc method, from a sensitivity point of view, or a dynamic method based on PC, will have difficulties providing the necessary short pulses and would pose much greater demands on the detection system. Another answer is related to a more fundamental aspect of the carrier lifetime and its relation to material parameters affecting recombination. This will be clarified below for modulated and quasi-steady-state-type methods. Dynamic methods are, therefore, explicitly described in forthcoming sections of the article.

Principles of the Modulation-Type Method

The principle can be demonstrated by an oversimplified model. Suppose the sample is irradiated uniformly by a harmonic modulated optical source at frequency ω with a generation intensity $I = I_0 + I_1 \exp(i\omega t)$, $i^2 = -1$. The concentration of minority carriers throughout the sample can easily be given from the continuity equation (Equation 1) under steady-state conditions, neglecting surface effects and nonlinear recombination terms. A solution can be presented of the form

$$\Delta n = \Delta n_0 + \Delta n_1 \exp(i\omega t) \tag{21}$$

where Δn_1 is complex (an expression of the fact that Δn and I have different phases). The expressions for amplitude and phase are

$$|\Delta n_1| = \frac{\tau I_1}{\sqrt{1+\omega^2\tau^2}} \quad \text{and} \quad \tan\varphi = -\omega\tau \tag{22}$$

The behavior of $|\Delta n_1|$ and φ are illustrated in Figure 9. It is clear that either parameter may be used to obtain τ when a physical quantity, which is related to the excess carrier density concentration, is measured as a function of modulation frequency. The sensitivity of the phase lag is high enough in the interval $0.1 < \omega\tau < 10$ since the phase lag is 45° at $\omega\tau = 1$. To obtain τ from the amplitude versus frequency curve demands measurements up to frequencies of at least a factor of 10 higher, that is, when $\omega\tau \sim 10$. Note that the effective lifetime τ' in a modulated measurement is given by

$$\tau' = \frac{\tau}{\sqrt{1+i\omega\tau}} \tag{23}$$

and the effective carrier diffusion length from the relation $L_D = (D\tau)^{1/2}$ follows as

$$L'_D = \frac{L_D}{\sqrt{1-i\omega\tau}} \tag{24}$$

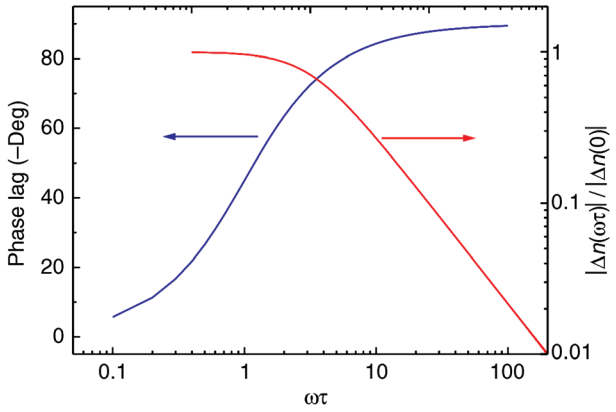

Figure 9. The frequency dependence of $|\Delta n_1|$ and φ as given by Equation 22, showing that both parameters may be used to measure carrier lifetime under harmonic modulation conditions.

This clarifies the principle of the modulation methods. The phase shift can be determined very precisely at a single selected frequency, using a narrow-band receiver and lock-in detection, thus separating noise problems, which are usually associated with a direct measurement of a transient response in any pulsed lifetime method. In practice, it is important to study both amplitude and phase shift over a wide frequency range in order to establish an appropriate regime, after which routine characterization may rely on a single measurement of phase shift at a moderately low frequency.

Principles of the Quasi-Steady-State-Type Method

From Figure 9, it also follows that if the modulation frequency varies very slowly compared to the effective lifetime, the phase lag approaches zero. In this case a quasi-steady-state condition is reached and the amplitude of the slowly modulated signal offers an expedient method for steady-state lifetime measurement. Under steady-state illumination, a balance exists between the generation and the recombination of electron–hole pairs. Expressing the photogeneration and recombination rates as photoinduced current and recombination current densities (J_{ph} and J_{rec}, respectively) it may be stated as

$$J_{ph} = J_{rec} \tag{25}$$

As a consequence of this balance, an excess concentration of electrons and holes is established in the material. The total recombination in a sample of thickness d can conveniently be expressed in terms of an average excess-carrier density Δn_{av} and an average lifetime τ_{av}, leading to:

$$J_{ph} = \Delta n_{av} q d / \tau_{av} \tag{26}$$

which, in essence, is a version of the classic relationship, $\Delta n = G\tau_{eff}$ (Ryvkin, 1964). For clarity, we state the classical analysis of the photoconductance, which, therefore, is a nearly direct way of probing the excess carrier

density. Equations 25 and 26 can be iterated to find the effective carrier lifetime as

$$\tau_{\text{eff}} = \Delta\sigma/[J_{\text{ph}}(\mu_{\text{h}} + \mu_{\text{e}})] \tag{27}$$

where μ_{e} and μ_{h} are corresponding mobility of electrons and holes. The conductance $\Delta\sigma$ and the incident light intensity should be measured using a calibrated instrument or a reference solar cell or photodiode, respectively. For a given illumination, J_{ph} can be estimated through available computer programs or lookup tables. In a typical 380-μm-thick silicon wafer with low reflection losses, the standard global AM1.5 solar spectrum produces a total photogeneration J_{ph} of $\sim$38 mA/cm^2 (AM1.5 standard reference spectrum defined in ASTME 892). The value of J_{ph} relative to the reference solar cell can be adjusted for a particular sample to take into account different surface reflectivities, sample thicknesses or illumination spectra.

Compared to a transient decay approach, the quasi-steady-state method allows a lifetime measurement without fast electronics or short light pulses. The range of measurable lifetimes is only limited by signal strength. Thus, the measurement is preferred for samples of low dark conductance. To measure very short lifetimes, the light intensity can be increased. Note, however, that the effective lifetime determined does depend on the details of the carrier distribution within the sample. The local excess carrier density is essentially equal to the average Δn_{av} obtained from Equation 26 when the surfaces of the sample are well passivated and the carrier diffusion length is greater than the sample thickness. In thick samples carrier density is better described by a weighted average, $\Delta n_{\text{av}} = \int_0^\infty \Delta n^2 dz / \int_0^\infty \Delta n dz$, over an effective width for the high concentration region, $W_{\text{eff}} = \left(\int_0^\infty \Delta n dz\right)^2 / \int_0^\infty \Delta n^2 dz$, see Bowden and Sinton (2007). It is also possible to find general steady-state solutions for the one-dimensional continuity equation subjected to boundary conditions of surface recombination in a semiconductor wafer (or in $n+p$ junctions) as, for example, expressed by Schroder (1990). The short-circuit current versus open-circuit voltage (I_{sc}–V_{oc}) characteristics can be equivalent to steady-state photoconductance measurements in solar-cell-type devices (Sinton and Cuevas, 1996).

It was established recently that minority carrier trapping can be extracted from apparent lifetime constant τ_a under the quasi-steady-state measurement. The following expression was used, Warta (2006):

$$\tau_{\text{app}} = \tau_R[1 + N_t/(\Delta n + N_t \times \tau_t/\tau_d)] \tag{28}$$

here τ_R is recombination lifetime, N_t is a given minority trap concentration, τ_t/τ_d is the ratio of minority carrier trapping/detrapping time constants as given by Equation 9 and Equation 17, respectively (Macdonald and Cuevas, 1999). This expression 28 follows from solution of differential equations for a free carrier in the bands and the occupation of a single trap level for the minority carrier. The model is applicable and has shown opportunities for trap parameters determination: a trap energy position and carrier emission cross-section can be extracted (Schmidt, 2002). Successive applications were obtained in multicrystalline Si solar cells, CZ-Si and in a number of cases. Quasi-steady mode approaches for μ-PC, PL and also for so-called infrared thermography were used (Giesecke et. al., 2011; Schubert et al., 2006; Ramspeck et al., 2008; Warta, 2006). Trapping effect can be suppressed under ll-injection condition by the application a strong sub-band gap light generation intensities, basically a bias-light, Warta (2006). Maps of trapping defect can be imaged.

Data Interpretation Problems

In practice, however, there are many cases where nonuniform carrier generation, surface recombination, nonuniform bulk recombination or nonlinear dependencies of recombination parameters introduce complications for both dynamic and quasi-steady-state methods. Serious problems arise due to existence of energetic barriers around traps or recombination centers in compound semiconductors. Moreover, lattice relaxation (the electron-phonon coupling) lead to change in the structure of the defect. For a specific energetically negative-U center there occur different defect charge state within the band gap. The specific nature of such amphoteric recombination centers were identified in Si, 4H–SiC, Ge and other semiconductors.

The problem can be further complicated by various sensitivity factors for detecting Δn_1. All these effects together imply that carrier diffusion currents at characteristic frequencies of the higher recombination terms (for modulated frequency $\omega\tau_{\text{i}}$) have to be considered. As a consequence, solutions for Δn_1 will be modified substantially. To calculate these expressions for the phase shift between the induced signal and the generation term, some kind of expression can be adopted. However, the resulting general expressions of carrier lifetime are too complicated to be useful.

A better procedure is to derive approximate expressions for the measured quantity by introducing various simplifying conditions in the steady state. Then, to make the appropriate substitution of τ' for τ (Equation 23) or L' for L (Equation 24), a number of expressions for modulated methods, where the algebra is reasonably tractable, is provided by Orton and Blood (1990). Specific microwave lifetime expressions by a harmonic optical generation method, which allows separation of the bulk lifetime and the surface recombination velocity on two wafer sides, are presented by Otaredian (1993). Currently, some decay measurements become converted to modulation measurement data and vice versa, since mathematical modeling procedures have improved considerably (Klein 2008; Ramspeck et al., 2008; Giesecke et al., 2011).

An even more complicated situation can appear if carrier bulk lifetime is determined by the distributed recombination levels in the energy band, as is the typical case in amorphous semiconductors. Some guiding

expressions for frequency-resolved modulated luminescence methods in amorphous semiconductors are provided by Stachowitz et al. (1995).

Summary of Strengths and Weakness

From the fundamental nature of the carrier lifetime and its relation to other material parameters, the strengths and weakness of different types of lifetime methods can be summarized as follows.

Quasi-Steady-State and Modulation-Type Methods. The major strength of these methods is that they provide a rapid and less complicated measurement. The lifetime may be obtained either from the amplitude or the phase lag of Δn. The equipment is typically inexpensive.

The major weakness of these methods is the complicated interpretation of the recorded data. In particular, this becomes important if a weak feature of the lifetime has to be extracted correctly. Interpretation in terms of injection-dependent recombination parameters is typically allowed in a limited range. The lateral resolution is determined by the carrier diffusion length (Ramspeck et al., 2008; Warta, 2006). Thermal heating of the sample should be taken in consideration under hl-injection.

Dynamic-Type Methods. As explicitly shown by examples in the following sections, the major strength of these methods is an adequate interpretation of the measurement results. Injection dependency of the lifetime and other related material parameters (carrier diffusivity, surface recombination) can be interpreted with the same algorithm. There is a large background of knowledge related to dynamic methods that has been developed over the past 40 years. Some of the equipment operating in narrow bandwidth range can be relatively inexpensive, while other methods can provide very sophisticated measurements with high lateral or depth resolution for the extracted lifetime.

The weakness of dynamic-type methods is that measurements typically require specialized equipment for working on different materials and in different bandwidth ranges. Dynamic techniques also are sensitive to background noise problems and reference standards must be used for quantitative measurements.

The impact of carrier trapping/detrapping impinges on the lifetime measurement. Complication arises if recombination of carriers in semiconductors takes place via several parallel recombination channels. The analysis of the experimental data intended to unravel the individual contributions is, however, often done on an intuitive basis rather than by a physically motivated formalism. The presumption $\Delta n = \Delta p$ is only valid for the case of perfectly symmetric capture rates of electrons and holes at recombination centers, and holds for high excitation conditions. Some authors claim that while this presumption is a reasonable approximation for steady-state conditions, it may lead to grossly erroneous results for transient conditions even in the limit of a small concentration of recombination centers (Brandt et al., 1996; Schüler et al., 2010). On the other hand, modeling of the transient shape makes possible the visualization of the evolution of carrier trapping quite easy (Ichimura, 2006).

FREE CARRIER ABSORPTION

The FCA method is a noncontact, fully optical pump–probe technique suitable for bulk lifetime measurements. It is based on optical injection of excess carriers, most often by a short laser pulse, and probing of the excess carrier decay by a continuous or pulsed wave. Usually an infrared beam is transmitted through the sample (Ling et al., 1987; Waldmeyer, 1988,). Yet, it is a quite universal technique, able to accommodate very different sample structures and semiconductor materials. The technique can also be easily set up in a research laboratory that has access to a pulsed laser of appropriate wavelength. So far, the technique has been extensively applied to indirect type semiconductors (Si, Ge, SiC, porous Si, GaP, $TlGaSe_2$, GaSe, etc.). The technique can also be applied for direct-type semiconductors like GaN, GaAs, CdS, etc. (Ščajev et al., 2011). Carrier lifetime studies can be executed also in semiconductor nanostructures which are dispersed in glasses (Kull et al., 1987) and in solutions (Yang and Kelly, 2006). However, in these cases the carrier lifetime extraction procedure should take into account interplay of FCA with the competing processes which is a dynamic bleaching above/near the bandgap energy range and absorption changes of impurity levels (below the band gap range).

Another advantageous feature is a possibility for good control of the injection level for FCA. This results from a homogeneous excitation volume, enabling a calibration of the carrier density. Thus, lifetime extraction may be performed at different injections probing different recombination mechanisms. This feature has inspired the selection of the FCA method as a demonstration unit to illustrate various concepts, as stated in the previous "Theory" section. For general reviews of the technique, see Linnros (Linnros 1998a, 1998b), Grivickas et al. (1992), Waldmeyer (1988), and Klein (2008).

Principles of the Method

The absorption of long-wavelength light induced by free carriers in a semiconductor, that is, for photon energies less than E_g, can be used to derive the carrier density in a sample. The absorption mechanism is related to acceleration of electrons and holes by the electric field of the incident radiation and generally increases with wavelength (Pidgeon, 1980). Elementary theory predicts a dependence of the absorption by semiclassical Drude model according to (for electron density *n)*

$$\alpha_{\mathrm{FCA}} = \frac{4\pi nq^2}{n^* cm^*}\left[\frac{\tau}{1+\omega^2\tau^2}\right] \tag{29}$$

where ω is the electromagnetic frequency, q the electron charge, c the velocity of light, n^* the real part of the refractive index, and m^* the electron (hole) effective mass, τ is the carrier relaxation time, respectively. For near optical wavelengths, $\omega^2\tau^2 \gg 1$, optical absorption

becomes proportional to the wavelength squared: $\alpha_{FCA} \sim \lambda^2$. In reality, different absorption mechanisms (phonon-assisted or allowed intraband optical transitions) may dominate and the quadratic dependence on wavelength should be replaced by a more general law. The most important consequence is the linear dependence of the absorption on carrier concentration, n.

For lifetime measurements, free carrier absorption may consequently be used to monitor the instant excess carrier density following optical injection of electron–hole pairs. As carriers are generated and recombine in pairs (assuming negligible trapping) it follows that the measured absorption is the sum of the contributions from electrons and holes, even though their individual absorption cross-sections may be different.

The transmitted probe beam intensity through a sample is described by

$$I(t) = I_0 \exp[-\alpha_{probe}(t) \cdot d]; \quad \alpha_{probe}(t) = \alpha_0 + \Delta\alpha(t) \quad (30)$$

where I_0 is the incident beam intensity, d the sample thickness, and α_0 a constant absorption coefficient related to, for example, dopant-induced free carriers. $\Delta\alpha(t)$ is the absorption coefficient, which is related to the density of **free excess carriers** within the sample. Usually, a linear dependence as in Equation 28 is assumed

$$\Delta\alpha(t) = \sigma_e \Delta n(t) + \sigma_h \Delta p(t) = \sigma_{FCA} \Delta n(t) \quad (31)$$

where $\Delta n(t)$ and $\Delta p(t)$ are the excess electron and hole time-dependent concentrations, respectively. In anisotropic semiconductor (like in hexagonal SiC polytypes) corresponding absorption cross-sections σ_e and σ_h depend on the polarization of the probe beam with respect to a particular optical axis in the crystal and the probe wavelength. Figure 10a shows measurements of $\Delta\alpha$ versus Δn in silicon for two temperatures and in Figure 10b the corresponding cross-section variation with temperature for two different probe wavelengths. The data in Figure 10a indicate a linear behavior. A slightly increased absorption at higher carrier concentrations is caused by an artifact from pump beam absorption enhancement.

In a general case, the carrier density may not be homogenous throughout the probed volume of the sample, and Equation 30 should be replaced by the average carrier concentration along the probe beam trajectory z within the sample, and a constant cross-section has been assumed as in Equation 31.

The pump beam photons generate free carriers in the form of electron–hole pairs, provided that the wavelength matches the fundamental absorption edge of the semiconductor sample. In the transient FCA method, the pump beam is represented by a short laser pulse. The carrier density depth profile can be calculated from the generation function described by

$$g(z,t) = g_0(t) \cdot \frac{\alpha_{exc}(1-R)^2 \exp(-\alpha_{exc} \cdot z)}{1 - R^2 \cdot \exp(-2\alpha_{exc} \cdot z)} \quad (32)$$

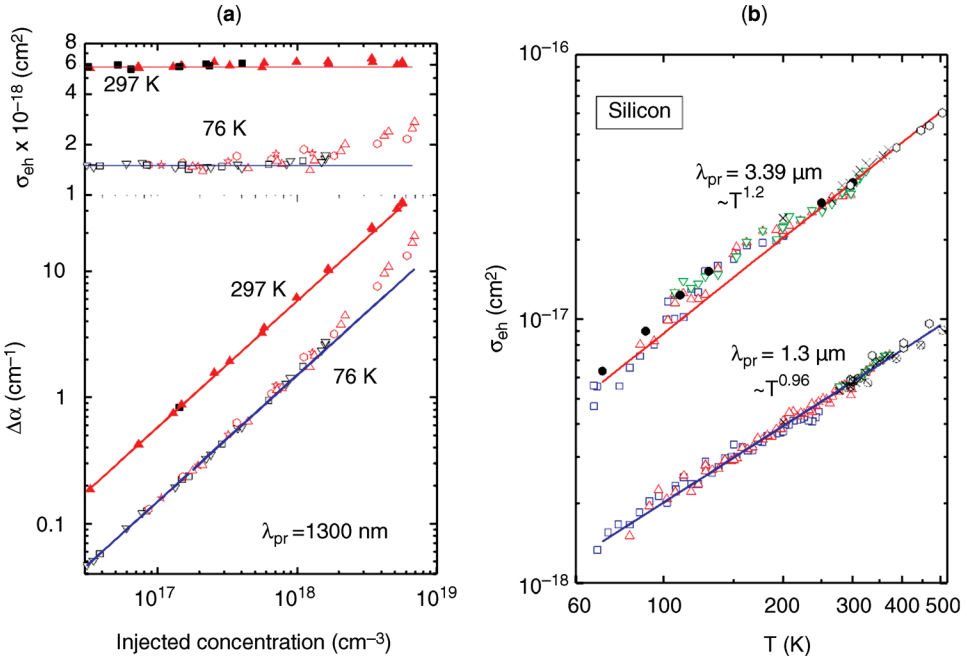

Figure 10. (**a**) Photoinduced absorption by excess carriers in silicon versus carrier injection for 1.3 μm probe wavelength at two temperatures; the top insert shows corresponding FCA cross-section. Band-to-band absorption is performed by 1.064 pump wavelength. (**b**) The temperature dependence of FCA cross-section for 1.3 μm and 3.39 μm probe wavelength. The excess carrier concentration was calculated using the absorbed optical power within a low doped sample of 500 μm thickness. Reprinted with permission from Grivickas et al. (2001).

where $g_0(t)$ is the incident flux density of photons, R the sample reflection coefficient (assuming equal reflectivity on front and back surfaces), and α_{exc} the absorption coefficient for the pump beam. An inspection of Equation 32 suggests that for an in-depth, homogeneously excited sample, $\alpha_{exc} \cdot d$ should be less than unity. Referring to the experimental data of Figure 4b, this condition is barely fulfilled in 4H–SiC epilayer, $\alpha_{exc} \sim 200\,cm^{-1}$ yielding $\alpha_{exc} \cdot d < 1$. (In contrary, the case of Figure 4a is an example of extremely opposite case of $\alpha_{exc} \cdot d \gg 1$ in Si for 532 nm pump wavelength).

Figure 11 left is a schematic of a *transient* FCA measurement setup using a *collinear* **beam crossing** geometry, that is, both excitation and probe beams enter the sample from the same side. The pump beam is pulsed and the excited area is large compared to typical diffusion lengths in the sample. The probe beam is from a continuous wave laser with a wavelength tuned toward the IR compared to the bandgap absorption which is in UV. By focusing, the probed sample area is smaller than the excitation area and may, therefore, be regarded as laterally homogenous. The transmitted probe beam is collected by a lens and focused onto a photoreceiver. To allow measurements on different areas of the sample, such as for lifetime mapping, the sample may be scanned in the plane of intersection of the two beams (e.g., by motorized translators; indicated by dot-line in Figure 11 left). The characteristic time for the FCA signal to revert to equilibrium is a measure of the carrier lifetime. Indeed, the temporal pulse width of the excitation laser must be short compared to the carrier lifetime of the sample in order not to affect the lifetime extraction.

An alternative geometry is the orthogonal setup (Grivickas et al., 1992; Linnros et al., 1993; Grivickas et al., 2000), shown in Figure 11 right, where the probe beam impinges on a cross-sectioned surface of a 4H–SiC epilayer sample, that is, at right angles with respect to the pump beam. This geometry enables depth-resolved measurements by moving the probe beam impingement spot on the cross-sectioned surface, or rather by moving the sample in the depth direction. This geometry allows lifetime depth-distribution (Fig. 4b), provided the epilayer is sufficiently thick that the probe beam may be focused and confined in this layer (Galeckas et al., 1997a).

In the selection between the collinear and the orthogonal geometry, one note that the collinear scheme results in a measurement of the average lifetime throughout a wafer (provided the penetration depth of the pump beam is large with respect to sample thickness). This is advantageous in many cases, such as during lifetime mapping. On the other hand, the orthogonal scheme provides a few other important advantages in addition to depth resolution. First, a uniform excitation is ensured along the beam path, even though excitation may be fairly inhomogeneous in depth. Second, samples may be cut in such a way that the probe beam path is quite extended, yielding a high sensitivity in terms of detected carrier concentration (refer to Equations 29 and 30, using a large d). This is often a prerequisite to reach low-level injection conditions.

Finally, a related method is the modulated-free carrier absorption technique (Sanii et al., 1992; Glunz and Warta, 1995) where, instead of a pulsed excitation beam, a modulated (usually sinusoidal) excitation beam generates carriers. The probe beam then monitors the resulting carrier modulation amplitude (or phase lag), which drops to zero (phase lag increases to 180°) at frequencies approaching the inverse lifetime ($f \sim 1/\tau$) as carriers are unable to follow the imposed modulation (see Section "Principle of the Modulation-Type Method").

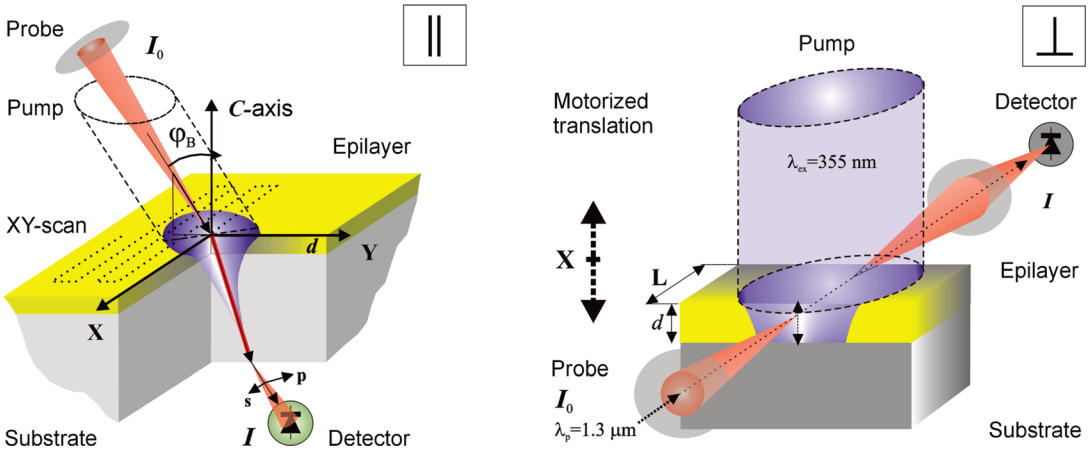

Figure 11. **(left)** Schematic of a pump–probe experiment to measure carrier lifetime in a collinear geometry on the 4H–SiC epilayer of thickness d grown on a substrate. Note that φ should be close to the Brewster angle to minimize multiple reflection of the probe beam. X–Y scan can be performed by moving the sample respect to the cross point of two beams as indicated. **(right)** Schematic of a pump–probe experiment to measure carrier lifetime in a orthogonal geometry for the same 4H–SiC epilayer. Depth resolved scanning can be performed by translating vertically the sample. (After personal permission by A. Galeckas).

Practical Aspects of the Method

Pump Laser Selection. For measurement of bulk lifetimes, a homogeneous excess carrier excitation in the sample is preferable to ensure the extraction of an in-depth average value of the bulk lifetime. As stated previously, this demands a relatively low absorption coefficient of the pump light, in turn requiring a photon energy close to the energy band gap. As an example, a yttrium-aluminum-garnet (YAG) laser operating at $\lambda = 1.06\,\mu m$ is ideally suited for Si wafers, as the absorption is $\sim 10\,cm^{-1}$, yielding a depth inhomogeneity of the initial carrier concentration less than ~30% for normal 350-μm thick wafers.

In contrast, when thin layers close to a semiconductor surface must be analyzed (in a orthogonal geometry as in Fig. 11), a higher absorption coefficient is desirable (Galeckas et al., 1997b). For 4H–SiC the wavelength of the third YAG harmonic $\lambda = 355\,nm$ is well appropriate, see Figure 4b, where the initial carrier concentration is given by the top profile α^{-1} (at $t = 0$). In such geometry, the part of the generated excess carrier profile penetrating into the substrate needs to be suppressed, requiring an excitation wavelength considerably shorter than for the previous case. One should keep in mind, however, that the result of such a measurement must be critically analyzed, since diffusion of carriers toward the surface and into the bulk becomes a more serious limitation as the thickness of the probed layer is reduced, and could seriously affect the measured carrier lifetime, Kimoto et al. (2010). In other words, the useful time domain of the expected lifetimes is pushed toward very short lifetimes, often into the ns or ps regime.

Finally, pulse duration and beam size must be considered. Whereas pulse duration must be kept below the shortest expected lifetime in the sample, minimum beam size should be at least a few carrier diffusion lengths in diameter. From practical aspects and ease of alignment, a diameter of a few millimeters is desirable, often necessitating the use of a beam expander.

Probe Laser Selection. The selection of probe laser wavelength is determined by sensitivity and focusing requirements. Generally, a high sensitivity is the primary requirement in speeding up lifetime measurements, in particular for lifetime mapping. As free carrier absorption increases with wavelength, longer wavelengths toward IR are preferable and the choice is often set by laser availability. For increased lateral or depth resolution, short wavelengths are advantageous. But, optimizing resolution is not a simple task, as the optical resolution is not set simply by the Airy-focusing spot size. Instead, the *effectively probed volume* in the sample determines the resolution as set by sample thickness, focusing lens, and wavelength. For a more detailed treatment, the reader is referred to Linnros (1998a). Finally, carrier diffusion most often sets the practical resolution, at least for indirect-bandgap materials with lifetimes in the microsecond range.

As probe lasers, HeNe lasers were traditionally used at operating wavelengths of 3.39 μm, 1.15 μm and 0.632 μm. Recently, light-emitting diodes (LEDs) have become abundant, offering several wavelengths in the visible and near-IR at affordable prices at 1.54 μm, 1.3 μm, or 0.86 μm, depending on band gap and the above selection criteria. When probing is performed using a delayed pulse from the excitation laser, the first harmonic pulse (1.06 μm) of the Nd:YAG laser usually is used together with higher harmonics of the YAG laser or from an optical parametrical oscillator, pumped by the excitation laser (Ščajev et al., 2011). Also, relatively intense tunable lasers have become available (100 mW) offering increased measurement speed, although care must be taken not to affect the carrier dynamics by probe beam heating.

Detection Electronics. The signal from the photodetector is normally amplified and subsequently fed into an oscilloscope. To reduce noise, it is important to limit the bandwidth to a minimum with respect to characteristic times as set by the detected recombination transients. This may most easily be achieved by reducing the bandwidth, an ability provided by most modern equipment. Even though transients might be observed by the eye on the oscilloscope screen, digital oscilloscopes are far superior, providing digital averaging on a large number of transients. In the selection of a digital oscilloscope, two features (besides analog bandwidth and sampling rate, which need to be compatible with expected lifetimes) are particularly important: (1) The ability to average detected transients into a 16-bit memory, providing greatly enhanced sensitivity span of FCA transients; and (2) an arbitrary offset bias on the input channel, offering the possibility to offset the steady-state I_0 value and increase the gain on the transient part of the signal.

Geometrical Considerations. To design the geometry of the setup, one needs to pay particular attention to interference effects of the probe beam within the sample. This results from the high index of refraction of semiconductors, yielding typical reflection coefficients of ~30%. For very rough surfaces, interference effects may be reduced, but in some cases (for normal Si wafers with nonpolished backside) the problem may still persist. The remedy is to lower the reflected part of the beam using a polarized probe beam and a Brewster angle geometry, as defined by $\tan(\theta_i) = 1/n_s$, where n_s is the semiconductor refractive index and θ_i the incidence angle. For depth profiling using the perpendicular geometry, the same holds for the probe beam entering the cross-sectioned surface of the sample as indicated in Figures 11.

Another practical important suggestion is that probe pulses, particularly those absorbed close to excited surface can generate acoustical wave which moves into the sample and can deflect the probe beam from the detector. This is a particularly important feature in a direct band gap semiconductor, where absorption above band gap exceeds values of $10^5\,cm^{-1}$. The desirable FCA measurements for different depths can resolve acoustical effects from a pure transient of FCA signal (Grivickas et al., 2007).

Method Automation

Computer Interfacing. The automation of lifetime measurements using the FCA technique is more or less mandatory, as the absorption transient may only be observed directly on an oscilloscope screen. The interface should have high data transmission capability, usually in the range of ~1 Mb/s, as found in modern instruments. A computer code to handle the reading of decay data may be written in any programming language and should be able to handle storage and presentation of data.

Lifetime Depth Profiling. For depth-resolved measurements (Linnros et al., 1993), computer control of a motorized micropositioner is needed. The micropositioner should be able to handle movements of good precision. The actual depth scan is performed by stepwise motion to the next position after the accumulation and readout of an averaged FCA transient. As focusing of the probe beam is crucial, the measurement is preceded by scanning the probe intensity across the depth. The fall-off of the intensity at sample edges is an indication of probe beam focusing.

Lifetime Mapping. Lifetime mapping demands automation and precision-motorized positioners in the two orthogonal scanning directions (Glunz and Warta, 1995; Linnros et al., 1995; Linnros, 1998b; Galeckas et al. 2001). As in the case of depth profiling, data accumulation and readout is followed by stepwise motion to the next position. The computer code controlling the mapping now becomes relatively sophisticated in order to optimize speed, data handling, selection of positions within the periphery of a wafer, and finally ease of handling for the user. The procedure for correct lifetime extraction is essential, as signal-to-noise ratio must be traded against measurement speed.

Data Analysis and Interpretation

Extraction of Carrier Decay Transient. The measured absorption transient, as recorded by a digital oscilloscope and transferred to a computer, may be transformed to a carrier decay transient using Equations 29 and 30 and solving for $\Delta n(t)$

$$\Delta n(t) = \frac{1}{\sigma_{\mathrm{FCA}}} \cdot \frac{1}{d} \ln \frac{I_0}{I(t)} \tag{33}$$

where α_0 now has been lumped together with I_0 as it represents a constant absorption during the measurement. To correctly define I_0, a few data points before the actual beginning of the pump pulse are needed. Also the representation of relative transmission $\ln[T_0/T(t)]$ can be equally used since it is proportional to the transient carrier density. Finally, sample thickness must be measured and an appropriate absorption cross-section must be inserted. However, to extract the lifetime, neither thickness nor cross-section is needed, as is evident from Equation 7.

Lifetime Analysis. The lifetime may be derived straightforwardly by applying Equation 7 with some numerical averaging profile over a few data points. An alternative route is by plotting $lg\Delta[n(t)]$ versus t followed by fitting of a straight line to some limited range of data points or simply using as an approximation the time where the FCA concentration is reduced to the level of $1/e$. The last case yields very fast data acquisition time, therefore, different recombination mechanisms may be not distinguished properly from the carrier decay transient.

In the illustrated case of Figure 12 a recorded absorption decay transient has been converted to excess carrier density. The measurement was made on a p-type Si wafer doped to $3 \times 10^{16}\,\mathrm{cm}^{-3}$ with boron, and a $\lambda = 3.39$-μm probe beam was used (excitation by a pulsed $\lambda = 1.06$-μm beam). To increase the signal-to-noise ratio, averaging of several thousand decays was performed at a repetition frequency of 40 Hz. This yielded a detection sensitivity of $< 10^{14}\,\mathrm{carriers/cm}^3$ (signal-to-noise level), as seen in the figure.

Analyzing the decay shape, one may distinguish three distinct regions. (1) At high injections nonexponential recombination is present due to Auger recombination (2), while at slightly lower injection, but still above the doping density, a linear region is observed where a high-injection lifetime may be extracted. Finally, (3) at low injections, the minority carrier lifetime may be derived. The inset shows a transient recorded at very high injection, where Auger recombination prevails.

In Figure 13, extracted lifetimes from the data of Figure 12 and a few additional recorded transients are displayed. Lifetimes were derived by a stepwise linearizing procedure of the data points in the transients. Solid lines represent a fit to the SRH formula (assuming a mid-gap trap energy level; see Equation 10 and Fig. 2),

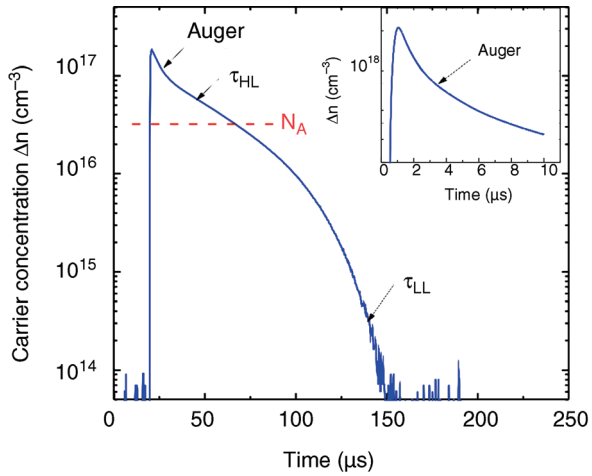

Figure 12. Excess carrier decay transients following an optical generation pulse in Si (p-type, $N_A = 3 \times 10^{16}\,\mathrm{cm}^{-3}$, thickness: $d = 430$ μm). The excess carrier density has been calculated using a linear cross-section (see Fig. 10), from absorption transients of a 3.39-μm probe beam. Inset demonstrates Auger recombination at high injections. Reprinted with permission from Linnros (1998a). Copyright 1998, American Institute of Physics.

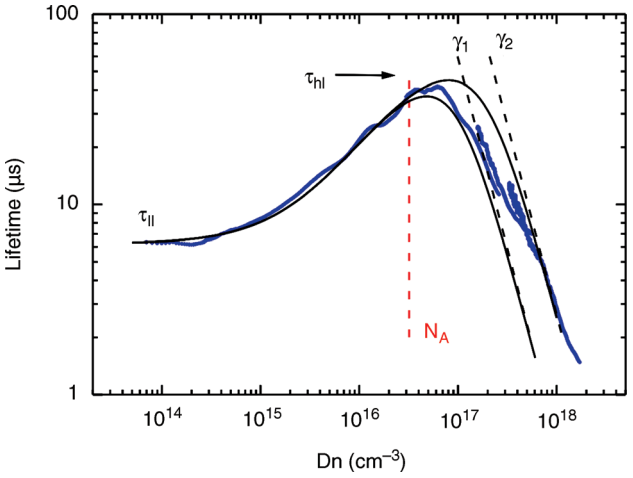

Figure 13. Calculated lifetime-injection dependence (solid circles) from experimental excess carrier decays as displayed in Figure 12. The two solid curves have been calculated according to the SRH theory (using Equations 10 and 16) assuming a minority carrier (electron) lifetime of 6 μs and a high injection lifetime of 60 μs, and for two Auger coefficients. $\gamma_1 = 1.7 \times 10^{-30}$ cm^{-6}/s and $\gamma_2 = 3.8 \times 10^{-31}$ cm^{-6}/s (from Dziewior and Schmid, 1977, and Grivickas and Willander, 1999, respectively). Reprinted with permission from Linnros (1998a). Copyright 1998, American Institute of Physics.

accomplished by varying the high- and low-injection lifetimes. Auger recombination is also included (see Section "Theory") where γ_1 and γ_2 represent two different Auger coefficients (Grivickas et al., 1996, Grivickas and Willander, 1999). One may note the good correspondence with theory and the broad transition range between the pure high-level (hl), low-level (ll), and Auger-injection case, complicating the interpretation of extracted lifetimes.

From the discussion above, one may conclude that the FCA technique allows a detailed study of carrier recombination at different injection levels, whereas an accurate determination of the minority carrier lifetime and/or the high injection lifetime may only be derived from plots similar to Figure 13 (by extrapolating to the pure ll or hl limit). In many cases, the lifetime may be estimated at a particular injection level, allowing comparison of the statistical spread of lifetime in different samples. Generally, the extracted lifetime value represents sample purity. The appropriate injection level for lifetime extraction depends on practical considerations (detection sensitivity) as well as on device applications for the analyzed sample/material. A tentative device may operate under high-level injection and, therefore, the hl-lifetime is of primary interest.

Analysis of Lifetime Mapping Data. Figure 14a show examples of lifetime maps for lifetimes extracted both in the epilayer and in the substrate of a 40 μm thick 4H–SiC 1″ wafer. This is done in order to exaggerate relations and important differences between these two cases since many fine-shape defects (dislocations, mocrotwins, etc.) from the substrate are grown into the 4H–SiC epilayer. The lifetime fit was performed using a fixed injection interval at the high injection lifetime. The mapping data have been displayed in the form of contour plots using the software.

Another example of a FCA lifetime map on a 3″ thick 4H–SiC wafer is shown in the middle of Figure 14b, Klein (2008). Here a comparison is also shown with two maps obtained from the same sample by the microwave photoconductivity (μ-PCD) and by the photoluminescence (TRPL) technique. A qualitative comparison between the lifetime distributions of the three techniques is seen. However, the average lifetime is 270 ns for PL, 600 ns for FCA and 700 ns for μ-PCD. Some of these results were obtained at different injection levels slightly below the hl injection. It is apparent that there is close similarity of the extracted average lifetime between the FCA and the μ-PC results but a factor of 2 shorter lifetime in the PL measurements. This will be discussed further in the PL section. It is clear that care must be taken to ensure that the same physical lifetime is being probed with the same environmental factors (injection level and temperature). Ideally, a surface recombination velocity map could be measured independently, although this is not always practical.

In cases where the lifetime distribution is too complicated to provide full lifetime mapping, an alternative simple representation can be performed—a statistical lifetime measurement and rough correlation of it with defects visualized by an optical microscope. An example is shown for the lateral segment of a freestanding 3C–SiC wafer given in Figure 14c at two temperatures, Here the stacking fault distribution is visualized in a cross-polarized Nomarski optical image.

Diffusion-Controlled Lifetime Data Interpretation. In the case of extended macroscopic defects of very high density propagating through the layers, there are specific relations between lifetime and defects. An important concept underpinning the diffusion-controlled mechanism is the relation between the size of the defect and the mean-free path of the carrier flow L_D. If the capture radius, d_{id}, ascribed to the defect, within which the capture probability is infinite (i.e., excess carrier density tends to zero), then the recombination rate will be diffusion controlled if $d_{id} > L_D$. If $d_{id} < L_D$, then the local depression of the carrier concentration is small and the carrier flow into the recombination centre is ballistic. This is underlying the assumption of the SRH recombination model (Equation 8) and is required to make the concept of a geometric capture cross-section valid. The switch between "diffusion" and "recombination" controlled lifetimes and its dependence on capture radius cannot be obtained by simple lifetime mapping since it is beyond the mapping resolution. In this case, a recommended procedure is to search for a lifetime correlation to the carrier diffusion coefficient, by looking to a temperature-dependent measurement. At hl-injection both values (lifetime and diffusion coefficient) can be determined by the transient grating technique. The technique is based on creation of a sinusoidal generation of carriers under a spot of irradiated area. The following grating decay time τ_G relationship is expressed

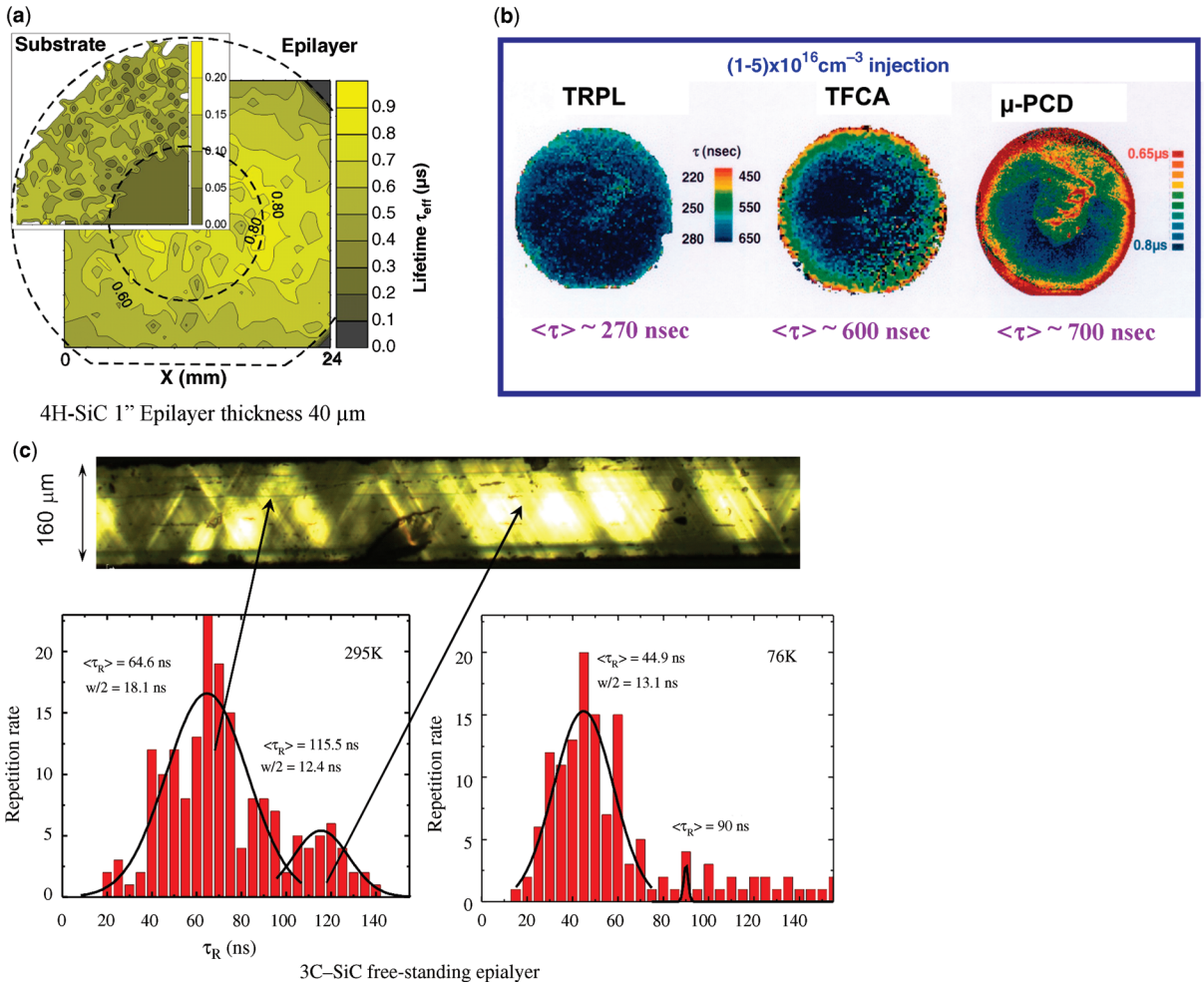

Figure 14. Examples of FCA carrier lifetime maps in SiC materials. (**a**) Effective carrier lifetime distribution in 40-μm thick 1" 4H–SiC epilayer at hl-injection. Insert shows the corresponding lifetime map on a quarter of the same sample heavily doped substrate. Note the enhancement of carrier recombination within a central region where N doping of the substrate exceed higher values. After Galeckas et al. (2001). (**b**) Carrier lifetime maps of 160-μm thick 3" 4H–SiC epitaxial wafer of doping $n_0 = 4 \times 10^{14}\,\mathrm{cm}^{-3}$ determined by time-resolved PL, FCA, and microwave PC (from the left to right). Injection level is $\sim 5 \times 10^{16}\,\mathrm{cm}^{-3}$. The average lifetime reflect important differences between three techniques used. After Klein (2008). (**c**) Carrier lifetime FCA distributions over cross-sectional part of 3C-SiC free-standing sample piece at two temperatures. Arrows show relation with different stacking faults defect distribution which is exaggerated by cross-polarized light image. The mean lifetime values and the statistical spread are indicated. Reprinted with permission from Grivickas et al. (2010). Copyright 2010, American Institute of Physics.

as $1/\tau_G = 1/\tau_R + 4\pi^2 D/\Lambda^2$, where Λ is the grating spacing period. By variation of Λ, both τ_R and D can be determined separately. The reading of the transient grating erasure may be performed either by a fine FCA scan across the grating (for $\Lambda > 50\,\mu$m fringes, Grivickas, 2004) or by probe beam holographic diffraction from the photoinduced refractive contrast on the grating fringes (for Λ ranging between 2 and 25 μm, Jarašiūnas, 2006). The last way is much faster and more appropriate. We note, that measurement by the transient grating is mostly important for D value definition since lifetime measurements by a standard FCA technique in a collinear geometry is simpler, reliable and more sensitive compared to the lifetime extraction from the transient grating decay where lifetime is obtained from the extrapolation of the result to $\Lambda = 0$.

Figure 15a shows the results obtained in hydride vapor phase epitaxy GaN layers of various thickness from 10 to 145 μm. A linear increase in nonradiative carrier lifetime in the 80-800 K range was found in correlation with a decrease of the bipolar carrier diffusivity in Figure 15b. This inverse correlation confirmed that the recombination rate is governed by a carrier diffusive flow to the grain boundaries as the threading dislocation density situated on boundaries dependent on the GaN layer thickness. A model for correlation with

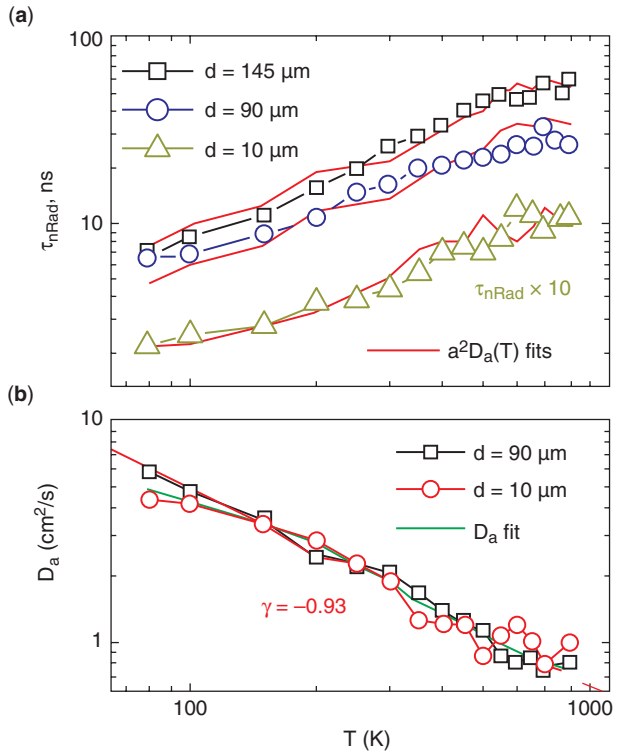

Figure 15. (**a**) Diffusion-limited nonradiative recombination lifetime versus temperature in epitaxy GaN layers of different thickness and (**b**) Its inverse correlation to temperature dependence of ambipolar carrier diffusion coefficient. Reprinted with permission from Ščajev et al. (2011). Copyright 2011, American Institute of Physics.

dislocation densities is given in Figure 16. Further numerical modeling has confirmed the observed inverse quadratic dependence of carrier lifetime versus TD density in thick GaN layers, see for details Ščajev et al. (2011). Similar inverse correlation of lifetime and carrier diffusivity was detected in a number of compound material samples.

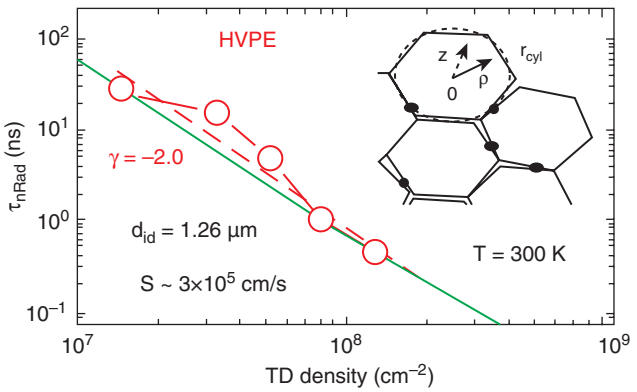

Figure 16. The lifetime dependence on screw threading dislocation (TD) density as in Figure 15. Points—experimental data, lines—fitted calculations. The insert in (**c**) shows the domain structure for modeling of the dislocations [the hexagonal prisms are rotated, dots indicate threading edge dislocations]. The used $s \sim 3 \times 10^5$ cm/s value is approximately 10 times lower than its theoretical limit, thus indicating that TD cover 10% of the grain boundary length $L_{GL} = d_{id}N_d$, and the corresponding effective dislocation radius is of $d_{id}/10 \approx 120$ nm. Reprinted with permission from Ščajev et al. (2011). Copyright 2011, American Institute of Physics.

Sample Preparation

Sample preparation ranges over the entire spectrum, depending on semiconductor material, surface properties, and measurement geometry. The listing below is structured according to different types of applications.

Virgin Wafers: Surface Passivation. To extract the bulk lifetime in virgin epilayers (for SiC, GaN wafers) is probably the most difficult task for any lifetime measurement technique. The reason is surface recombination in combination with a large defect density. The problem arises also for the manufacturer specification for lifetimes on measurements on boules before cutting into wafers.

There are a couple of approaches to circumvent surface recombination problem. This may be performed by a low-temperature chemical passivation process (Linnros, 1998b; Yablonovitch et al., 1986), or by other chemical methods (Horanyi et al., 1993). An alternative is to charge the native oxide of a Si wafer with ultraviolet UV light (Katayama et al., 1991) in order to provide band bending that will prevent carrier diffusion to surfaces (see center panel of Fig. 3). Common to all these methods are, however, problems with stability and repeatability.

Naturally, for SiC wafers or other semiconductors with short carrier lifetimes, the problem of surface recombination is reduced, but, it still needs to be carefully addressed. Finally, an optical problem may arise for wafers/samples with nonpolished backsides as this may spread the probe beam such that the detector signal vanishes. In such cases it is necessary to polish the backside.

Processed Wafers and Devices: Removal of Metal and Highly Doped Layers. In many cases, processed Si wafers are excellent for measurements of the bulk lifetime using the FCA technique. The reason for this is that furnace processing in Si often results in a surface oxide, which may provide a very low surface recombination velocity. Another advantageous case is when dopants are diffused from the surfaces. This results in p–n junctions, nn^+- or pp^+-junctions that serve as barriers for carrier diffusion toward surfaces (see right panel of Fig. 3). For highly doped emitters, however, the probe beam may be completely attenuated by the high permanent concentration of carriers in these layers. A solution would then be to either remove this layer partly (by etching or polishing) or by decreasing the absorption using a shorter probe beam wavelength. For devices, metal layers must be removed to ensure transparency to pump and probe beams.

Depth Profiling: Cross-Sectioning of Samples. For depth-resolved measurements using the perpendicular geometry, a cross-section must be cut from the wafer/sample. Special attention has to be paid to the parallelism of the surfaces and to the thickness of the cross-section. The latter determines the obtainable depth resolution and a

graph for simple estimations for Si samples may be found in Linnros (1998a). Using a good cutting machine with a diamond blade, however, a mirror-like surface may be obtained. Polishing should be performed using conventional procedures.

Problems

As for most carrier lifetime measurement techniques, surface recombination is one of the main problems. This results from carrier diffusion, and the critical parameter is the diffusion length of carriers in comparison to sample dimensions. For short carrier lifetimes, the effects of surface recombination may be smaller. On the other hand, one may be interested in carrier lifetimes of thin films or epilayers, and surface or interface recombination may again be a limiting factor.

The diffusion length also limits using the technique for local lifetime determination, as, for example, in the top surface region of active devices. In such cases, one needs to resort to lifetime techniques based on generation lifetime as in a depleted p–n junction.

A specific problem with the FCA technique is the determination of minority carrier lifetime under very low injection conditions, as needed for wafers with low levels of doping. This is due to the limited sensitivity of optical absorption techniques at low carrier concentrations. The sensitivity may be optimized using large samples, long wavelength probing, and extended averaging. In silicon, sensitivities of $\sim 10^{11}$ carriers/cm^3 have been reached (Grivickas et al., 1992) although the injection level during lifetime mapping is, for practical reasons, limited to $\Delta n \sim 10^{15}\,\mathrm{cm}^{-3}$.

Another problem, although very rarely encountered, is the measurement of extremely long carrier trapping lifetimes. In such cases, a large excitation spot is needed to reduce effects of radial outdiffusion of carriers from the excited area (Linnros, 1998a).

PHOTOCONDUCTIVITY

The measurement of PC decay in various experimental modifications is widely used as a convenient method for measuring carrier lifetimes in semiconductors. As an example, the archetypal method of PC-decay under a constant current applied by means of ohmic contacts has been set as a standard technique for measurement of the minority carrier lifetime in bulk germanium and silicon for >40 years (Standard Method for Measuring the Minority-Carrier Lifetime in Bulk Germanium and Silicon, F28 in ASTM, 1987). Numerous noncontact PC methods, such as microwave reflectance and rf bridges, have recently become quite popular because their nondestructive quality and also their suitability for use in a clean-room environment. Most of the considered techniques do not require particularly expensive and bulky instruments. This motivates the wide diffusion of noncontact PC decay techniques into diverse areas of carrier lifetime measurements including on-line processing of silicon wafers.

Principle of PC Decay Methods

The principle of the experiment involves shining a pulse of light into the semiconductor sample to generate excess carriers and monitoring the time decay of the corresponding excess conductivity. Since electrons and holes have opposite charge, the total conductivity is the sum of the partial conductivities, which is positive. Consequently, conductivity can be written in the form

$$\Delta\sigma(t) = q[\Delta n(t)\mu_n + \Delta p(t)\mu_p] \cong q\Delta n(t)[\mu_n + \mu_p] \qquad (34)$$

where q is the electron charge and μ_n, μ_p are the corresponding drift mobilities of electrons and holes, respectively, that characterize PC for different injection levels.

Before proceeding to details, it is worthwhile to reiterate two general points. First, the simple case when both Δn and Δp are equal in time and in the unit volume. Numerous experiments have shown that misbalance effects can be neglected for lifetimes in the range 1–500 μs of crystalline Si and Ge (Graff and Fisher, 1979). However, we note that the approximate equality often does not hold for some highly irradiated, highly damaged crystalline semiconductors, polycrystalline or amorphous films (Brüggemann, 1997). The indeterminate cases may appear in compound semiconductors, particularly in compensated materials. In the following, we shall assume that the approximate equality in Equation 34 is an inherent property. This assumption leaves complicated interpretation of PC transients out of the scope of this article.

Second, it has usually been assumed that the PC decay process senses the carrier concentration decay where mobilities are constant parameters. Such an assumption may be made in the great majority of actual cases. However, this cannot be true at high injection where electron–hole scattering reduces mobility substantially, for example, in high-resistivity Si (Grivickas et al., 1984) and at cases of carrier trapping. A few papers have also reported that the carrier mobility was changed during PC transients in high-resistivity polycrystalline and compound semiconductors because of the effective recharging of scattering clusters. We do not attempt to provide an exhaustive accounting for these effects and we shall assume that the decay of excess carrier concentration is always controlled by minority carriers through SRH recombination and either by a direct band-to-band or an Auger-type recombination mechanism.

Practical Aspects of the Standard PC Decay Method

By the standard technique, PC decay is monitored through the change of sample conductance in a constant electric field. Current is passed through a monocrystalline semiconductor specimen by means of ohmic contacts. The experimental arrangement in its simplest form is shown in Figure 17. The sample is bar-shaped with dimensions of typically $l \gg d, w$ and has ohmic contacts on its end faces. The light beam is oriented normal to the applied electric field (a case of transverse PC). The intensity decreases with depth in the sample according to Beer's law. Neglecting multiple reflection, the

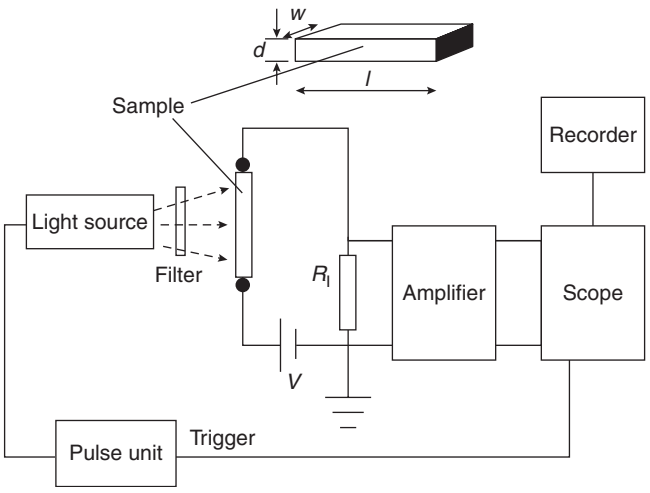

Figure 17. Basic experimental setup for photoconductive decay measurements in a constant electric field. Excess carriers are monitored as an increase in sample conductance.

photoconductance of the whole sample can be obtained (Ryvkin, 1964) as

$$\begin{aligned}\Delta G &= (w/l)q(\mu_n+\mu_p)\, I_0[1-\exp(-kd)] \\ &= (w/l)q(\mu_n+\mu_p)\int \Delta n\, dx\end{aligned} \tag{35}$$

where I_0 is intensity penetrated from the front surface of the sample and k is the absorption coefficient. For sufficiently thick samples $kd>1$ all light energy is absorbed in the sample and the photoconductance is independent of the absorption coefficient. Therefore, in this case the carrier distribution in the x direction is highly inhomogeneous.

In addition to the transverse PC (Fig. 17), the longitudinal PC is sometimes investigated. In this type of experiment, a semitransparent electrode is illuminated with the light beam parallel to the field. In general, the longitudinal case has a more complex relationship with fundamental semiconductor parameters. We confine our discussion in this article to transverse photoconductivity.

As shown in Figure 17, the sample is connected in series with a battery supplying a voltage V and a load resistance R_L. Consequently, interrupting the light, the current in the circuit has a constant component and an alternating one. The voltage drop may be monitored with an oscilloscope by a signal average between the ohmic contacts (or between a second pair of potential contacts in a four-terminal measurement). In general, the voltage drop is monitored by the load resistance R_L. A rather complex relationship between the alternating voltage received at the amplifier input and the variation of ΔG can be expected under the action of light. In special cases, this relationship is simpler (Ryvkin, 1964). For example, if a small load resistance is used, $R_L \ll (G_0+\Delta G)^{-1}$, where G_0 is the equilibrium conductance, then the relationship is linear because the illumination does not greatly alter the electric field distribution in the sample and the load resistance. This case sometimes is called the *constant field* regime. The resistor must be nonreactive, with a resistance at least 20 times less than that of the sample in the excited state, to provide a condition of essentially constant field. As described by Ryvkin (1964), two other regimes, such as the *constant current* regime, $R_L \gg (G_0+\Delta G)^{-1}$, or the *maximum-sensitivity* regime, $R_L=(G_0)^{-1}\ [1+\Delta G/G_0]^{-1/2}$, can be frequently used. While the last two regimes, in general, do not imply proportionality between the signal and ΔG, a linearity is obtained when the relative change of the photoconductance is small ($\Delta G/G_0 \ll 1$). Thus, a constant current regime is recommended for minority carrier lifetime measurements in bulk Si and Ge by the ASTM standard F28 (ASTM, 1987).

The threshold of ΔG measurement sensitivity depends on various types of noise superimposed on the measured signal and the type of recording instrument. The minimum detectable photoconductance is also governed by the value of the equilibrium conductance, G_0, other conditions being equal (Ryvkin, 1964).

PC Method Automation for High-Frequency Range

Ordinary PC transient measurements are quite restricted on a nanosecond time scale because capacitance and/or induction of conventional electrical circuit elements produce failure effects. PC lifetime measurements in the 1–25 GHz frequency range are developed through strip-line techniques by driving so-called microline switches (Lee, 1984). Coplanar metal waveguides are monolithically integrated on the semiconductor sample to provide characteristic impedance $\sim$50 Ω, with a corresponding spacing (photoconductive gap) a few micrometers wide. Free carriers can be generated in the gap by fs-laser pulses and accelerated in an applied bias field, producing an electrical transient. The output of the circuit is measured via high-frequency connectors attached to the strip lines by a fast sampling oscilloscope. Lifetime resolution down to picosecond's range can be achieved.

Sampling experiments can also be performed without the need for an expensive fast oscilloscope. In this case, two photoconductive switches, one serving as a gate and having a very fast response function, can be connected in parallel and excited with delayed optical pulses. The temporal profile of an incident signal voltage pulse, $v_{sign}(t)$, can be measured by scanning the time delay, Δt, between the signal pulse and the gate pulse. The sampling yields a dc current given by the signal correlation

$$I(\Delta t) = \int v_{sign}(t) f_{samp}(t-\Delta t)\, dt \tag{36}$$

where f_{samp} is the known sampling function corresponding to the optical gate pulse. Inexpensive lock-in amplifiers can measure dc currents, provided that colliding optical pulses are chopped at low frequency. The lifetime can be estimated from mathematical simulations of the correlation function $I(\Delta t)$. The time resolution is limited by the duration of the sampling function of the gate

switch. The ideal sampling function is a delta pulse, and, in fact, this has motivated the fabrication of a gate switch made from semiconductor materials with reduced carrier lifetime in a subpicosecond range (Smith et al., 1981). Therefore, the gate sample in this case should be regarded as a distributed circuit element, and the propagation of the wave through the photoconductive gap should be properly treated (Lee, 1984). Four factors have been shown to be of special importance. These are the free carrier lifetime, local dynamic screening, velocity overshoot, and the carrier transient time from the photoconductive gap (Jacobsen et al., 1996).

High-frequency measurements usually involve high excitation levels and high electric fields. In these cases, carrier recombination is affected by fundamental processes of carrier momentum randomization, carrier thermalization, and energy relaxation in the bands (Othonos, 1998). At very high injections, PC in semiconductors usually obeys a nonlinear dependence as a function of light intensity. The most probable cause of nonlinearity in a photoconductor is related to carrier lifetime. Pasiskevicius et al. (1993) have proposed to use PC correlation effects for measuring nonlinearities in ultrafast photoconductors. In this way, correlation signals are recorded on a single switch using a double pulse excitation scanned relative to one another. A peak will be observed on the autocorrelation traces when the photocurrent is a superlinear function of optical power and a dip when this function is sublinear. The widths of these extrema will be determined by the duration for which the switch remains in the nonlinear state.

The typical experimental setup used by Jacobsen et al. (1996) is sketched in Figure 18. Colliding pulses (100 fs) of a mode-locked Ti:sapphire laser are divided into two beams, with one beam passing through a delay line. Both beams are mechanically chopped and focused onto a biased photoconductive switch, and the relative arrival time is varied by mechanically moving the delay line. The current flowing in the photoconductive gap is measured by using a current-sensitive preamplifier, and the signal is sent to a lock-in amplifier. The preamplifier operation is slow compared to the time scale of the carrier dynamics, so a time average of the current is measured. In order to suppress noise, the two beams are chopped at different frequencies f_1 and f_2, and the lock-in amplifier is referenced to the difference frequency $|f_1 - f_2|$. In this way, the correlation measurement integrates only the product of the carrier density and the local electric field that corresponds to both pulses. Therefore, a rapid recharging of the photoconductive switch is required by a short recombination lifetime. Lifetimes as short as 200 fs have been measured using this correlation scheme.

Additional information on PC processes can be obtained from a set of compatible electrooptic techniques based on Pockels, Kerr, Franz–Keldysh effects, as reviewed by Cutolo (1998).

Detailed protocols of minority carrier lifetime determination in bulk Si and Ge by a classical PC technique are provided in F28 in the Annual Book of ASTM Standards (ASTM, 1987). Other applicable documents of ASTM Standards are E177 [Recommended Practice for Use of the Terms Precision and Accuracy as Applied to Measurement of a Property of a Material (ASTM, 1987, Vol. 14.02) and F43 Test Methods for Resistivity of Semiconductor Materials (ASTM, 1987, Vol. 10.05)].

The specimen resistivity should be uniform. The lowest resistivity value should not be <90% of the highest value (see Test Methods F43; ASTM, 1987). The precision expected when the F28 method is used by competent operators in a number of laboratories is estimated to be better than ±50% for minority carrier lifetime measurements on Ge or ±135% for measurements on Si, as defined in Recommendation Practice E177.

A similar, but not equivalent method is under the responsibility of Germany DIN Committee NMP 221. This is DIN 50440/1, Measurement of Carrier Lifetime in Silicon Single Crystals by Means of Photoconductive Decay: Measurement on Bar-Shaped Test Samples. This document is available from Beuth Verlag GmbH, Burggrafenstrasse 4-10, D-1000 Berlin 30, Germany.

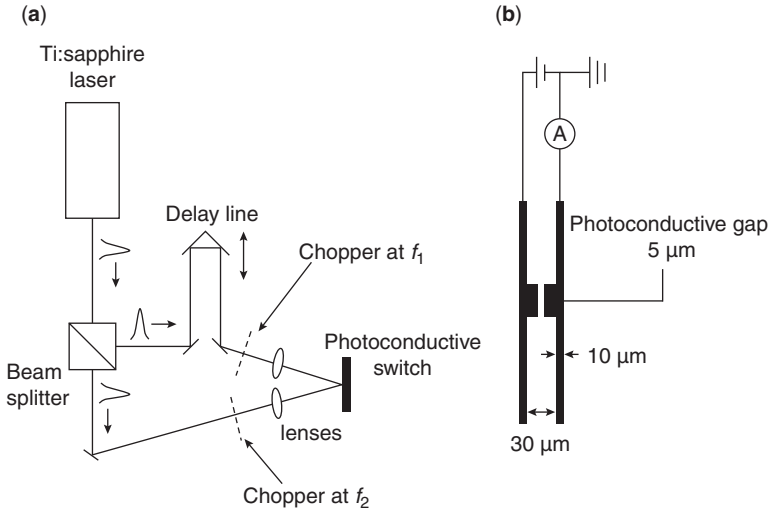

Figure 18. (**a**) The experimental setup for the photocurrent autocorrelation measurements in subpicosecond range. (**b**) Antenna design used as a photoconductive switch. The laser spot is focused in the 5-μm gap in the middle of the transmission line. Bias is applied across the gap and the current is measured. Reprinted with permission from Jacobsen et al. (1996). Copyright 1996, American Institute of Physics.

Data Analysis and Related Effects

For reliable interpretation of the experimental data by the standard PC method, it is important that the measuring electric field E be uniform throughout the sample. This implies the use of good ohmic contacts, and it is also necessary for contacts to cover the whole area of the end faces. Also, the sample cross-section and resistivity must remain constant over the sample length. Another requirement is that the magnitude of the electric field be low, such that the injected carrier density is not disturbed by excess carrier sweepout. The appropriate criterion can be obtained applying a drift term to the continuity equation (Orton and Blood, 1990). This leads to the condition

$$(\mu E)^2/4D \ll \tau_{\text{ef}}^{-1} \tag{37}$$

where D is carrier diffusion coefficient. If $\mu = 10^3\,\text{cm}^2\,\text{V}^{-1}\,\text{s}^{-1}$ and $\tau_{\text{eff}} = 1\,\mu\text{s}$, and applying the Einstein relation, $D = k_{\text{bt}} \cdot \mu/q$, for the carrier diffusivity, this results (at 300 K) in the requirement that E should be much less than 10 V/cm. It is advisable to check experimentally that a change in E has no effect on the measured decay time.

Another possible source of error lies in the generation of photovoltages at the contacts if these are not ohmic. The signal should be observed without applied voltage in order to determine the magnitude of such a photovoltage. The amplitude of any photovoltaic signal should be less than 1% of the desired photoconductive signal. Also, the same PC amplitude with applied voltage must be observed for both polarities of the constant-voltage source. If the specimen voltages for the two polarities agree to within 5%, the contacts may be considered as nonrectifying. All connections to the contacts should be made with shielded cables, which must be as short as possible. The requirements for the performance of the preamplifier should be considered together at the same time. For working in the small-signal regime, it is advisable to mask contacts and illuminate only the central part of the semiconductor bar (F28, ASTM, 1987).

For the measurement of minority carrier lifetime, a finite injection level is required under low-level injection conditions. This level can be obtained by the standard PC measurement technique from the ratio of the voltage change, ΔV, across the illuminated specimen, to the voltage, V, across the specimen when the specimen is not illuminated. When the ratio $\Delta V/V$ is restricted to < 0.01, the corrections to the lifetime value may be ignored. When the modulation of the measured voltage across the specimen exceeds 0.01, a correction is required to find the minority carrier lifetime, τ_{ll}. From the voltage decay time, τ_v, which is the quantity actually measured, a correction to the minority carrier lifetime is recommended as determined by the following equation (F28, ASTM, 1987)

$$\tau_{\text{ll}} = \tau_v[-(\Delta V/V)] \tag{38}$$

Sample Preparation

The largest possible specimen should be used, to minimize the contribution of surface recombination to the observed lifetime value. By the method description in ASTM Standard F28 (ASTM, 1987), it is also recommended that surface effects be attenuated. Specimen surface can be sandblasted or ground to produce a reference surface for which a limiting high surface recombination rate may be calculated (see Equation 20 and Fig. 5). It is recommended that the corrections applied to an observed filamentary specimen lifetime never exceed the observed value. That is, the condition for low level-injection lifetime, $\tau_{\text{ll}} > \tau_b/2$, should never be violated. Tables 3 and 4 show the maximum values of the bulk lifetime, τ_b, which may, therefore, be determined on three standard small-sized specimens according to the F28 method.

Although many methods may be used for making contact connections (e.g., diffusion or implanted n^{++} or p^{++} layers), it is suggested by F28 that pressure contacts of metal braid or metal wool can be used for measurements at low injection. Thick sheets of Pb or In have also been found to be acceptable for this purpose. The ends of Ge specimens should be plated with either Ni, Rh, or Au. Nickel plating is satisfactory on the ends of n-type Si specimens and rhodium plating on the ends of p-type Si specimens. Copper should be avoided in the plating operation. Electrical contacts formed by alloying with an Au–Sb–Si eutectic can be recommended for PC measurements on n-Si at high-injection levels (Grivickas et al., 1984).

Different technological procedures for minority carrier lifetime retention in Si wafers—before and after thermal heat treatment in various atmospheres, as well as after chemical treatments, after final deionized water rinsing, etc.—have been presented with respect to minority carrier lifetime analysis by Blais and Seiler (1980), Graff and Pieper (1980), and Graff and Fisher (1979).

Microwave PC Decay Method

A wide range of alternative PC decay methods exist, which have the advantage of not requiring electrical contacts to the sample. Most popular is the sensitive method of measurement the fractional change in the microwave power *reflected/transmitted* from the sample. Due to the plasma effect, the dielectric constant of the semiconductor is a function of excess conductivity. A variety of experimental arrangements is possible depending on available microwave frequencies: for

Table 3. Dimensions of the Three Small-Sized Filamentary Specimens for which Limiting Bulk Lifetime Data are Presented in Table 4

Size Designation	Length (cm)	Cross-Section (cm)
A	1.5	0.25×0.25
B	2.5	0.5×0.5
C	2.5	1.0×1.0

Table 4. Maximum Values of Bulk Lifetime, τ_b, in μs, for the Three Size Designations in Table 3, as Recommended by the F28 Photoconductivity Method for Minority Carrier Lifetime Measurements at 300 K

Material	Size A (μs)	Size B (μs)	Size C (μs)
p-type Ge	32	125	460
n-type Ge	64	250	950
p-type Si	90	350	1340
n-type Si	240	950	3600

example, through strip line systems (1–4 GHz), or through *X*-band (8–12.4 GHz), or through the *Ka*-band waveguide apparatus (28.5–40 GHz). The choice can be made between transmission or reflection systems, the use of a resonant cavity, or geometrical configurations within a partially closed system or outside it (see Ahrenkiel and Dunlavy, 2011). A number of laboratories use a microwave reflector behind the sample to produce a double pass of the microwave probe from the lower conductivity samples. Some methods are described by Orton and Blood (1990). Commercial apparatus for microwave reflectance lifetime measurements are also available and works best with planar structures.

A usual approximation to the time-resolved microwave signal change $\Delta P(t)/P_0$ is given by

$$\Delta P(t)/P_0 = A \cdot \Delta\sigma(t) \tag{39}$$

where A is called the **sensitivity factor** and is given by

$$A = \left(\frac{1}{R'(\sigma_0)}\right)\left(\frac{\partial R'(\sigma_0)}{\partial \sigma_0}\right) \tag{40}$$

where A is nonlinear to resistance and can be determined by measuring R' for different values of dark conductivity, or calculated from electromagnetic theory (Kunst and Beck, 1988; Otaredian, 1993; Swiatkowski et al., 1995). A comprehensive calculation of reflection coefficient (or a quality power of the coupled circuit) and conductivity sensitivity functions [10^{-5} to 10^{1} $(\Omega\ \text{cm})^{-1}$ range] for frequencies $f = 0.1 - 100$ GHz has been provided by Otaredian (1993).

The sensitivity factor is usually set to be proportional to the square of the microwave electric-field strength, $A \approx E^2(z)$, then the sample is placed at a maximum of the standing microwave. Reference to sensitivity resolution leads one to consider the question of the skin depth, which determines the depth of material actually monitored by the microwave probe. At 10 GHz, skin depth is ~500 μm for a conductivity of 1 $(\Omega\ \text{cm})^{-1}$ and varies approximately as $(\sigma_0 \times \text{frequency})^{-1/2}$. As quantitatively shown by Swiatkowski et al. (1995), the decay process has to be interpreted with care for the intermediate dark conductance range and in cases of higher injection because of the inhomogeneous excess photoconductivity in the z direction. In general, for higher conductance samples, data acquisition at lower microwave frequency is preferred (Ahrenkiel and Johnston, 2008). The technique has been successfully applied to thin films grown on substrates (Ahrenkiel and Dunlavy, 2011; Klein 2008).

A number of researchers extended the microwave method to obtain minority carrier lifetime maps over whole semiconductor slices by mounting the sample on a positioning table. Spatial resolution may be obtained by focusing the light beam to a small spot or by monitoring the local resistivity with a small microwave probe. The measurement is very rapid and requires minimal tuning and adjusting. A lateral resolution of < 100 μm is possible and a typical lifetime as short as 40 ns. In modern case, a few nanosecond can be achieved (Ahrenkiel and Dunlavy, 2011.

Problems

Microwave PC setups in Si are basically maintained to minority carrier lifetime regime (ll-injection) conditions because of the nonlinear conductivity–reflectance relationship. For SiC this range exceed somehow into at relatively higher injection of $10^{16}\ \text{cm}^{-3}$. There is usually a limited range of carrier decay span.

Radio Frequency PC Decay Method

In the radio frequency (rf) method, rf bridges, operating in the 10–900 MHz range, have been implemented for monitoring transient PC of semiconductors. The basic idea of the technique is that a semiconductor sample can be coupled to a rf bridge without the need for actual physical wire contact. Either inductive coupling by a 2–5 turn radio coil (Yablonovitch and Gmitter, 1992) or capacitive coupling by two flat electrodes (Tiedje et al., 1983) can be utilized. In effect, the coil or the capacitor is the primary of the transformer circuit and the semiconductor wafer is a secondary. The rf apparatus monitors the absolute sheet conductivity of the semiconductor, both in quasistatic and in dynamic modes. The circuits are designed to digitize the reflected rf signal due to the impedance imbalance caused by the sheet conductivity changes in a semiconductor when the light is on. Small conductivity changes in the semiconductor will only perturb the tuning, and the reflected rf wave from the primary circuit will be linearly proportional to sheet conductivity. The output bridge signal is then mixed with an adjustable phase-shifter signal of the same frequency to give sum and difference output components. The difference component is a signal that is detected and recorded using an oscilloscope. Because there is no direct contact with the sample, electronic measurements can be performed both in aqueous media as well as in a vacuum. More recently, a sophisticated technique of resonance-coupled PC was developed in 400–500 MHz range by Ahrenkiel and Johnston (2003).

The measured quantity is proportional to $\Delta\sigma$ where the constant of proportionality can be found by calibrating the detection circuit with semiconductor wafers of known conductivity (Tiedje et al., 1983). In general, a higher frequency increases the sample signal and also gives the circuit a better time response to monitor changes of the sample's conductance. While the skin depth is lower at lower frequencies, at 100 MHz it allows

the electromagnetic radiation to penetrate even highly doped samples of 10 $(\Omega\ \text{cm})^{-1}$ to a thickness of a few hundred microns. Lateral resolution of the lifetime by the rf method is, however, quite limited due to the large area of coupling, and is of the order of several mm^2. A carrier lifetime as short as 40 ns can be measured.

Problems

All PC decay measurements suffer from the following limitations.

1. It is very difficult to obtain separate quantitative information on the electron and the hole density alone, since both are equally present in the total PC. Partial conductivities may be obtained only in some specific cases. Such cases appear in damaged (amorphous) semiconductors at low injection levels (see Section "Trapping").
2. Carrier mobilities are always weighting factors for the PC decay. In known cases, it is recommended an algorithm that corrects for the mobility injection variation.
3. In addition, for noncontact PC the sensitivity factor A and the proportionality factor must be properly calibrated, usually for each material and for dark conductance of the sample. Linearity of these constants should be checked and maintained in PC transients. None of the PC techniques function well when a metal back contact is a component of the sample.
4. Except for the microwave technique, where local resolution is possible, only integrated lifetime over a relatively large area of the excited material can be represented by the PC decay.
5. While PC can be utilized in either a near-surface or bulk excitation mode, the main problems (as in any volume-integrated measurement) are the precise knowledge of the injection level and separation between surface and bulk contributions.

PHOTOLUMINESCENCE

Measurement of minority carrier lifetime in direct bandgap semiconductors and in nanostructures is usually performed by the PL technique, since emission yield is rather high. This is a nondestructive and noninvasive measurement that is very time-efficient. For process control and evaluation, one can measure lifetime in a simple structure and evaluate its performance. The individual components of multiple epitaxial layers can often be separately probed where only small quantities of material are needed. The lifetime, the diffusion length, and the quantum efficiency could be inferred. The main advantage is based on the fact that PL is an optical spectroscopic technique, that is, it gives energetically resolved information. In particular, it is sensitive to the chemical species of impurities, which can be detected even at very low densities. This motivates the wide diffusion of this technique in the field of materials science and solid-state physics.

Principles of the PL Method

The PL decay method measures the radiation emitted by a material after optical excitation; in other words, it monitors various radiative recombination paths of photoexcited electron–hole pairs. The transient decay of the PL signal is called the PL lifetime. When combined with a model of the transient response, which is derived from the continuity equation, the minority carrier lifetime and other recombination lifetimes are calculated. The principle of the experiment is very simple: excess carriers are injected by an appropriate light source in their fundamental absorption band, and the corresponding emission range is selected by a suitable monochromator and detected by a photoreceiver. The photoluminescence spectrum can usually be divided into three main energy regions whose width depends on the particular material. The numbers quoted in the following are characteristic of direct gap semiconductor crystals, for example, GaAs of $E_g = 1.43$ eV.

Near-Bandgap Emission ($E_g - 2E_{\text{ex}} < \hbar\omega < E_g + 2\text{kT}$, *where* E_{ex} *is the exciton-binding energy*). In this region, interband transitions, free and bound exciton recombination, and bound electron-free hole transitions are observed. At room temperature and above, exciton and shallow donor-related luminescence is thermally quenched. Band-to-band recombination dominates the spectra, and the PL edge position can even be used to determine the alloy composition of compound semiconductors such as $Al_xGa_{1-x}As$ (Pavesi and Guzzi, 1994).

Shallow Impurity Emission ($E - 200\,\text{meV} < \hbar\omega < E_g - 2E_{\text{ex}}$). In this region, hydrogen-like shallow impurity related recombination is present. The information that one obtains from luminescence in this region also reflects the chemical species of the impurities involved in the transition, their relative densities, compensation ratios, etc.

Deep Level Luminescence ($\hbar\omega < E_g - 200\,\text{meV}$). In this region, the recombination of deep impurities and acceptor–donor defects PL is observed. Bound exciton to deep impurity also is observed. The study of low-energy luminescence also gives information on important properties of the crystal such as stoichiometry, nonradiative recombination channels, stacking fault, dislocation defects, etc.

The radiative band-to-band recombination rate R of free electrons and holes (Fig. 1) is given by

$$R = B \times pn(\text{cm}^{-3}\text{s}^{-1}) \tag{41}$$

Here p and n denote total concentrations of holes and electrons. The B-coefficient is specific to a particular semiconductor and is proportional to the dipole matrix elements between the conduction and valence band wave functions. This coefficient can be established by calculation from the integrated absorption spectrum using the detailed balance relationship (Van Roosbroeck and Shockly, 1954). Therefore,

experimentally determined B coefficients are much larger for direct than for indirect band gap materials and have quite different temperature dependencies. For example, B is $2 \times 10^{-10}\,\mathrm{cm}^3/\mathrm{s}$ for GaAs and $\sim 10^{-14}\,\mathrm{cm}^3/\mathrm{s}$ for Si at 300 K (see Table 1).

From Equation 12, the low-injection radiative lifetime is

$$\tau_{\mathrm{RAD}} = 1/(BN) \tag{42}$$

where N is the doping or majority carrier density. In many cases, at N of $10^{17}\,\mathrm{cm}^{-3}$, the radiative lifetime is about 50 ms and is orders of magnitude larger than the typical SRH lifetime. Consequently, faster SRH competing processes determine the carrier lifetime and dominate the observed PL decay; $I_{\mathrm{PL}}(t)$ tracks $\Delta p(t)$ in time. Thus, the band–band PL under low-injection conditions should follow the minority carrier concentration decay and reflects minority carrier lifetime. Under high excitation conditions, instead, $I_{\mathrm{PL}}(t) \approx B \times \Delta p(t)^2$. Consequently, the PL intensity decays twice as fast as SRH hl-lifetime, due to the bimolecular recombination kinetics. This is confirmed by averaged lifetime values experimentally observed in 4H–SiC (Fig. 15b), where comparison is made of the PL lifetimes with the PC or the FCA lifetimes; both last ones are obtained from decays which is directly proportional to carrier concentration. However, the photoluminescence decays with the minority carrier lifetime only when there is no charge flow out of the active volume. This is why PL decay is useful for qualitative analysis, but is not a reliable measurement tool for minority carrier lifetime exact values in crystalline silicon wafers. Here overlap of impurity-activated transitions with the intrinsic band–band transition is a primary source of the scatter, Ahrenkiel et al. (2007). A more accurate measurement is therefore obtained from confinement structures which prevents carrier diffusion loss, such as from $n+/n/n+$ AlGaAs-type heterostructures (Ahrenkiel, 1992).

Practical Aspects of the Method

It is important to recognize that the external PL decay $I_{\mathrm{PL}}(t)$ measures the overall minority carrier lifetime, not the radiative lifetime, because, in general, the recombination rates add as given by Equation 16. All nonradiative recombination paths (e.g., via deep recombination centers) compete with the radiative process in the bulk of the semiconductor and also with surface (or interface) recombination (see Section "Theory") in the context of the decay concept. It is convenient to note that the internal efficiency defined as the ratio of radiative to total recombination rate, can be expressed in terms of Equation 43

$$\eta_{\mathrm{i}} = \frac{\tau_{\mathrm{eff}}}{\tau_{\mathrm{RAD}}} = \tau_{\mathrm{eff}} BN \tag{43}$$

For a steep absorption edge and high emission efficiency, the reabsorption of the photons generated by radiative recombination, termed *photon recycling*, leads to an increase in both the lifetime and the diffusion length of minority carriers. This behavior produces an apparent increase in radiative lifetime in GaAs type heterostructures which, for an active layer thickness d, can be written in terms of a photon recycling factor $\phi(d)$ as

$$\tau_{\mathrm{eff}}^{-1} = \tau_{\mathrm{nonRAD}}^{-1} + [\phi(d)\tau_{\mathrm{RAD}}]^{-1} \tag{44}$$

where τ_{nonRAD} is the bulk minority carrier nonradiative lifetime. The parameter $\phi(d)$ is a complicated function of the internal radiative efficiency, the critical angle for total internal reflection, and the absorption coefficient, and can only be calculated numerically.

From Equation 44 it is clear that influence of reabsorption is minimal if nonradiative lifetime is much shorter than the radiative lifetime. This condition is almost always valid in indirect semiconductors (Klein et al., 2011) and, in many cases (moderately doped, nonpassivated) for direct semiconductors as well, allowing a simple interpretation of PL dynamics. Figure 19 shows an example of PL-detected nonradiative carrier lifetimes in n-GaAs under shock wave compressions. In these experiments, extreme longitudinal stresses up to 4 GPa are produced along desired crystal orientation by impacting them with accelerated projectiles during a state of uniaxial strain before sample starts to break. Time-resolved PL measurements are recorded in single event experiments under short temporal window by using a spectrometer, a streak camera and a CCD detector and 200 ps pulse excitation.

Application to Nanostructured Semiconductors

The PL method is widely used for characterizing nanostructured or low-dimensional semiconductors. This is largely because a main interest is the characterization of

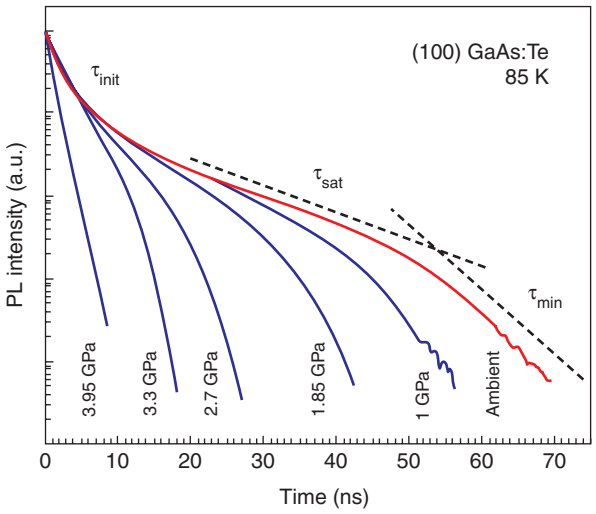

Figure 19. SRH lifetime injection dependences obtained by spectrally integrated PL measurement under shock uniaxial strain compression at different longitudinal stresses in GaAs:Te. Hl-lifetime (τ_{sat}) and ll-lifetime (τ_{min}) is indicated by dashed lines. 532 nm pulse laser excitation. Reprinted with permission from Grivickas et al. (2011). Copyright 2011, American Institute of Physics.

the PL energy—that is, spectroscopy, which enables characterization of the semiconductor bandgap which may shift from its bulk value due to quantum confinement. The confinement can then be in one dimension—*quantum well*, in two dimensions—*quantum wire* or in all three dimensions – *quantum dot* (also named nanocrystal). Another reason for the extensive use of PL in nanostructure characterization is that electrical methods are usually difficult due to problems of contacting and due to poor current transport in nanostructured materials.

Lifetime characterization of nanostructured materials using the PL method can be achieved using the same equipment as for bulk characterization provided sufficient volume of the material is available. Characterization of individual nanostructures—such as a single quantum dot, on the other hand, is much more complicated and will be treated in a following section. While PL lifetime methods used for bulk materials may also be used for *ensemble* studies of nanostructured materials, these materials may not be homogeneous having size dispersion on the nanometer scale. As a consequence, bandgaps may vary causing an inhomogenous line broadening of the PL spectrum. Thus, these materials are by themselves inhomogeneous and PL spectroscopy and lifetime measurements yield then average characteristics as sampled by their absorption of the pump beam and by the reabsorption of the emitted PL. Using a spectrometer as a wavelength filter, one can, however, reduce the size dispersion at least in principle. This is based on the assumption that quantum confinement is related to the radius of the quantum dot thereby yielding a unique PL energy for a certain dot size.

In Figure 20 we show an example (Linnros et al., 1999) of PL lifetime measurements for silicon nanocrystals embedded in oxide. These nanocrystals have diameters

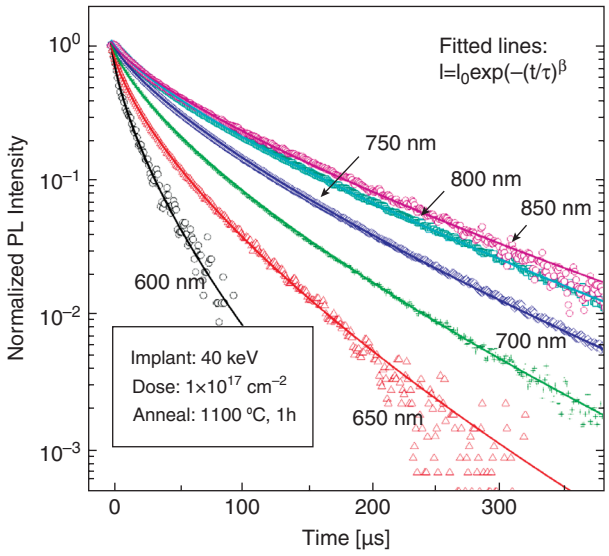

Figure 20. Time resolved PL decays ($\lambda_{exc} = 355$ nm) normalized to initial PL yield at each wavelength for a nanocrystal sample with a Si implanted and annealed SiO_2 film. Solid lines are stretched exponential fits to the decays. Reprinted with permission from Linnros et al. (1999). Copyright 1999, American Institute of Physics.

in the range 2–5 nm and quantum confinement increases their bandgap significantly compared to that of bulk silicon. Here PL decays have been recorded at different wavelengths in their fairly broad PL emission spectrum (peak emission at ~700 nm). As silicon is still considered to be an indirect bandgap material for these small sizes, decays are relatively long with lifetimes of the order of 100 μs. Moreover, shorter wavelengths (smaller structures) display faster decays which is indicative of a larger electron–hole overlap (higher oscillator strength for the dipole transition). The individual decays are, however, not described by a single exponential function but may be fitted by a stretched exponential function: $I = I_0 \exp(-(t/\tau)^{\beta})$ where the dispersion factor β in this case varies in the range 0.4–0.8. The origin of this stretched exponential can result from a sum of PL from somewhat different nanocrystals yet emitting at the same emission wavelength. Another alternative would be a random delay time introduced during individual decays as when a quantum dot goes into a nonluminescing state. This has been shown for single quantum dot decays by comparing with on/off intermittency of quantum dots (blinking). Indeed, for quantum dots which display relatively few blinking events single-exponential decays are observed while for dots which are sparsely on, decays are much more stretched [Schlegel et al. (2002); Fisher et al. (2004)], see Figure 21.

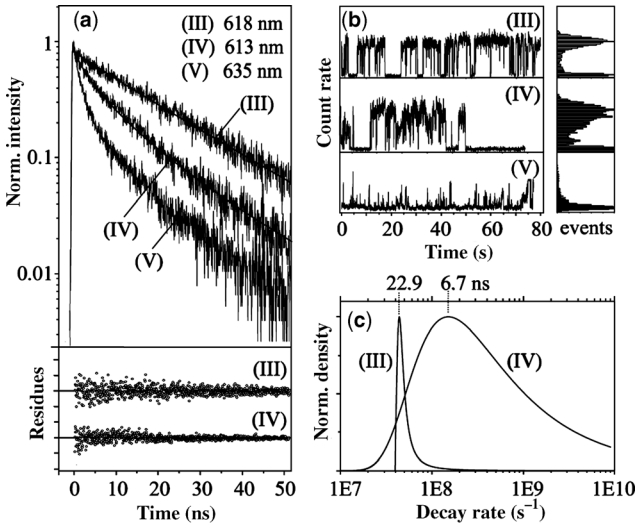

Figure 21. (**a**) Fluorescence decay curves of three different individual nanocrystals [(III), (IV), and (V)]. The decay curves of (III) and (IV) are fitted with a stretched exponential function revealing multiexponential dynamics. (**b**) Fluorescence transients and count rate histograms for (III), (IV), and (V) recorded at the same time as the decay curves in (a). Particle (III) shows a defined on-level with a maximum count rate of 200 counts/20 ms. The count rate distribution is much broader for particle (IV) while particle (V) fluoresces only periodically. (**c**) Distribution of fluorescence decay rates as calculated from the stretched exponential fit functions in (a). The almost single exponential decay of (III) results in a narrow rate distribution ($\tau_{max} = 22.9$ ns), whereas the strong bending of logarithmic decay curve from particle (IV) correlates with a broad rate distribution ($\tau_{max} = 6.7$ ns). After Schlegel et al. (2002).

Method Automation

The experimental setup complexity is proportional to the needs; for characterization, a very simple and cheap apparatus is sufficient. The earlier references describe a number of techniques (Orton and Blood, 1990; Schroder, 1990). Most workers have used short pulses from a laser or light-emitting diode (LED) to generate excess carriers. Alternative methods of excitation are also possible, the most popular being the injection from a metal contact or a p–n junction. The so-called cathodoluminescence decay method differs only in the use of a pulsed electron beam or x-ray as the excitation source.

An advanced technique for measuring photoluminescence decay with a high sensitivity and a fast time resolution is called time-correlated single-photon counting (Ahrenkiel, 1992). In order to use this technique, the photodetector must be able to detect single photons produced by the emitted light. The typical commercial photodetectors with sufficient sensitivity for photon counting are cooled photomultiplier tubes or microchannel plates (MCP). The transient time is greatly reduced in an MCP down into the picosecond range. The photodetector is followed by a high-speed amplifier, which is connected to the photon counting apparatus. A schematic of the experimental setup is shown in Figure 22a. The photons emitted by the sample are focused on the input slit of a scanning monochromator tuned to the appropriate wavelength. The time-correlated photon counting electronics are identical in the remainder of the detection system. Using a beam splitter and a photodiode, a small fraction of the excitation pulse is deflected to a fast photodiode. The electric output of the photodiode triggers the time-to-amplitude converter (TAC). The pulse-height discriminator is necessary to block electrical pulses produced by thermal and other nonphotonic sources. The first collected PL photon initiates an electrical pulse in the photodetector, which is passed by the amplitude discriminator. The electrical pulse produces a stop message at the TAC. The TAC output is a ramp generator with amplitude proportional to the time delay between the laser pulse and the arrival of the first photon. The TAC signal is fed to a multichannel pulse-height analyzer (MCA), which collects one count per detected photon. A count is stored in a channel appropriate to the time delay and a maximum of one count is recorded for every laser pulse. In this way, a histogram of the PL decay is built in terms of counts versus time.

Many different techniques have been used for obtaining time resolution in luminescence spectroscopy (Fleming, 1986). While some photodetectors can be made with much faster response times than a typical photomultiplier of ~50 ps, their low sensitivity restricts their use in detecting weak signals. Another technique, preferred for obtaining time resolution in the 1–100-ps range, has been to use a streak camera. Some single-shot streak cameras offer a time resolution of better than 1 ps in certain cases. However, a drawback is the spectral response of the photo-cathode, which typically does not extend beyond ~900 nm.

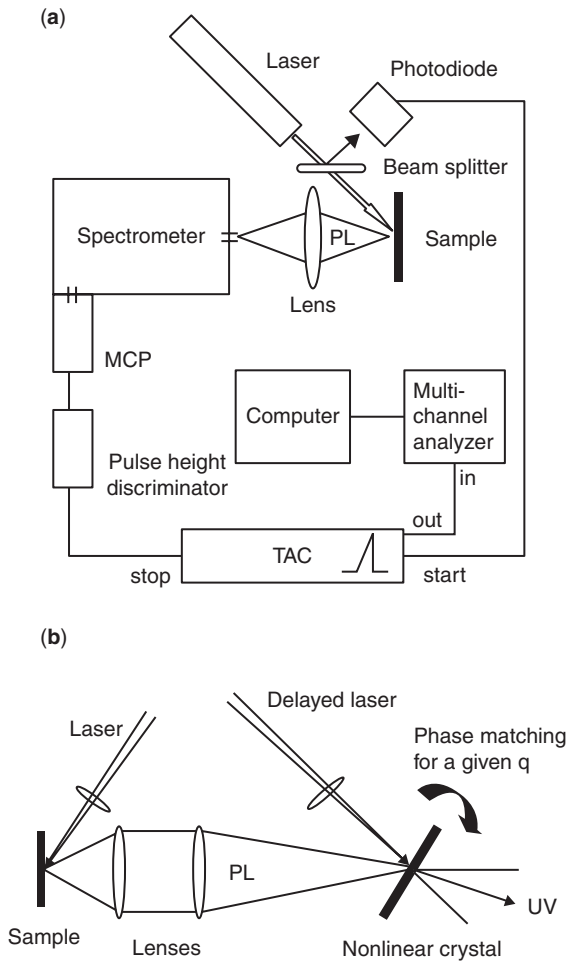

Figure 22. (**a**) Schematic of the PL decay measurement apparatus with time-correlated single-photon counting. Reprinted from Ahrenkiel (1992), Copyright 1992, with permission from Elsevier. (**b**) Schematic arrangement for the collection of luminescence for up-conversion. Sum frequency radiation is generated in a nonlinear crystal. After Shah (1988).

The best hope for achieving luminescence time resolution comparable to today's available lasers of fs pulse width appears to be techniques that use nonlinearity induced by the laser pulse as a gate for recording the luminescence. In this technique, the luminescence excited by an ultrafast laser is mixed with the laser in a nonlinear crystal [$LiIO_3$, (β-BaB_2O_4, CS_2)] to generate sum or difference frequency radiation, see Figure 22b. Since the mixing process takes place only during the presence of a delayed laser pulse, this provides time resolution comparable to the laser pulse width, as given by the experimental implementation of Shah (1988). Sum frequency generation, also known as wavelength up-conversion, is widely used because the availability of excellent photomultipliers in the visible and UV spectral regions makes this technique extremely attractive for time-resolved luminescence spectroscopy of infrared luminescence.

Single Dot Spectroscopy and Lifetime Characterization

Single-dot spectroscopy is a technique which originally came from studies of single molecules, (Moerner and Fromm, 2003) and then was applied to studies of single quantum dots. Most well studied have been the colloidal quantum dots from the II–VI system, Empedocles et al. (1996) such as CdSe, CdS, ZnS, PbS, PbSe, etc., but also self-organized InAs or InP quantum dots, grown on GaAs, have been used (Zwiller et al., 1999). The difficulties of observing single quantum dots stems from the weak luminescence from a single dot and techniques to disperse the dots sufficiently apart with respect to optical wavelengths used. Thus, it should be possible to measure the PL from an individual dot without interference from neighboring ones. In practice, this means a spacing between adjacent dots of at least a few microns. This case is illustrated in the schematics of Figure 23a where the dispersed quantum dots are imaged by a high-numerical aperture objective lens of magnification 50–100 X. In Figure 23b–d, on the other hand, a single quantum dot is selected from more closely spaced dots using either a small aperture fiber tip (in a scanning near field optical microscope), a hole in a deposited metal mask or by the electric field enhancement due to a conductive AFM tip, respectively. Finally, Figure 23e depicts the geometry of a confocal microscope where an inserted pin hole ensures that excitation and emission overlap in a certain probe volume. This suppresses noise and is particularly useful for more three-dimensional objects like cells or molecules in a liquid phase.

To record the weak luminescence from a single quantum dot, the experimental conditions must be carefully planned:

1. A high-numerical aperture (>0.80) objective lens must be used (when imaging a sample in a cryostat special correction lenses have to be used to avoid distortion by the cryostat window).
2. A short-wavelength cut-off filter should be used to suppress light from the excitation source. The source should also be cleaned from luminescence at other wavelengths using appropriate filters.
3. The PL system must be mechanically stable such that drift and vibrations are kept below 1 μm to prevent blurring of any quantum emitter. This puts restrictions on the type of cryostats used: Closed-cycle cryostats can normally not be used, although new models have come to the market in which the sample is vibrationally isolated from the cooled part in the cryostat.
4. Detectors used must have very low background noise. For spectroscopy, cooled CCD cameras are often used and for temperatures below $\sim -80^{o}$C one may expect background count rates of ~ 1 count/h per pixel.
5. For time-resolved measurements, avalanche photo detectors may be used which can reach down to ~ 1 count/s. The detected count rate from the analyzed quantum source must then be significantly higher than this.
6. Photomultipliers, gated image intensifier cameras, and streak cameras may be used for time resolved measurements provided that the studied sources are sufficiently bright to overcome the normally much higher background noise of these detectors.
7. Stray light must be eliminated requiring optical shielding of the system as well as operation in a dark room.

Data Analysis and Interpretation

A model case of an n-type semiconductor with excess injected carriers ($\Delta n = \Delta p$) exceeding the doping density, N_D, will be analyzed here as an example. In contrast to previous analyses (see description in the "Theory" section), we assume here that SRH recombination and radiative recombination are the only two main recombination channels that have to be considered in direct-bandgap semiconductors. From Equations 7 and 10, it follows that the instantaneous lifetime becomes (Ahrenkiel, 1992)

$$\frac{\partial I}{\partial t} = \frac{I + I^2}{\tau_p[1 + I] + \tau_n I} \tag{45}$$

where the instantaneous injection level is $I = \Delta p(t)/N_{\mathrm{D}}$ and the SRH electron and hole lifetimes τ_n, τ_p are

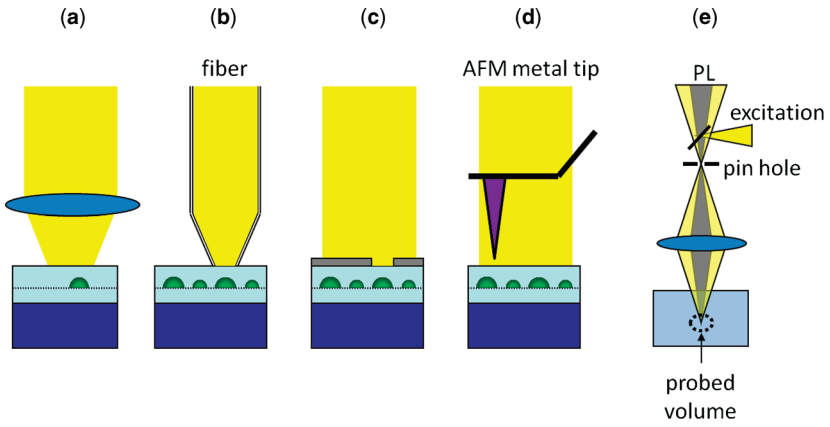

Figure 23. Methods for PL characterization of single quantum dots. (**a**) PL imaging, (**b**) scanning near field optical microscopy (SNOM), (**c**) nano patterning by metal mask or mesa etching, (**d**) tip-enhanced near-field imaging, and(**e**) confocal microscopy (for explanations see text).

described by Equation 9. The decay rate is nonexponential over an appreciable range of excess hole densities. One can fit the decay with these asymptotic rates and then define the initial injection ratio used in the experiment. The characteristic downturn of the decay curve has been seen in numerous devices and is an indicator of SRH recombination. When surface or interface recombination is the dominant mechanism (in thin devices), the photoluminescence decay may be fit with a function of Equation 45, replacing electron and hole lifetimes with the corresponding effective lifetimes: $\tau_{sp} = d/(2s_p)$ and $\tau_{sn} = d/(2s_n)$. The quantities s_p and s_n are interface recombination velocities for holes and electrons, respectively (refer to Equations 19 and 20). By varying the active layer thickness d, one can determine if the dominant recombination mechanism is bulk or surface related.

If a substantial concentration of excitons is present in a semiconductor at low temperatures, the PL decay becomes quite complex. The exciton level population should be included in the analysis as governed by the rates of formation and dissociation of excitons. Some description can be found in Orton and Blood (1990) and in Itoh et al. (1996). Usually, a strong coupling condition between the free exciton level and the conduction band can be used as a starting point.

In disordered materials (such as amorphous, polycrystalline, or porous semiconductors) the PL decay and lifetime is usually represented either by a stretched-exponential or a power-law line shape. Physical interpretation of effective lifetimes or a characteristic distribution of lifetime parameters, however, very much depends on the particular assumptions for the recombination and transport models (Stachowitz et al., 1995; Roman and Pavesi, 1996; Linnros et al., 1999; Klein et al., 2011.

Problems

From the discussion above, PL also has some disadvantages that can be summarized as follows:

1. It is very difficult to obtain quantitative information on the lifetime-doping-density relation or the lifetime-trap-concentration relation by PL alone. Some efforts, however, have been made in this direction, but the proposed methods require very accurate calibrations, checking very carefully the line shape of the spectrum (Schlangenotto et al., 1974; Pavesi and Guzzi, 1994; Ahrenkiel et al. (2007).
2. Photoluminescence provides information on radiative transitions. Only indirectly can one study the nonradiative recombination processes, essentially by analyzing the quantum efficiency.
3. Photoluminescence is not a bulk characterization technique, as briefly explained above. Only a thin, near-surface region can be investigated, defined roughly by the larger of the light penetration depth and minority carrier diffusion length.

SUMMARY AND SELECTION GUIDE

The three lifetime characterization methods described in more detail in this article—free carrier absorption (FCA), photoconductivity (PC), and photoluminescence (PL)—have in common optical generation of excess carriers by a pulsed light source. Their common advantages may be summarized as:

1. They offer the possibility of controlling the injection level, Δn, by varying the laser pulse energy (enabling the minority or the high-injection lifetime to be studied).
2. They offer the possibility of localized measurements by focusing the excitation beam.
3. They are versatile techniques that may be used for several different semiconductors.
4. They are contactless techniques (except for the direct PC technique) allowing simple (or no) sample preparation.

Their disadvantages may be summarized as:

1. They may yield erroneous lifetime values when carrier trapping is dominant (in this case a modulated or quasi-steady-state variant of the technique may successfully be applied).
2. Carrier diffusion and surface recombination may dominate recombination and, thus, the sought-after material parameter such as minority carrier lifetime or high injection lifetime may not be evaluated (as true for almost any lifetime measurement technique).
3. They require relatively complex experimental setup and knowledge.

Tables 5–7 compare the different methods reviewed in this unit, and may be used as a selection guide for

Table 5. Application of Selected Dynamic Lifetime Techniques for Characterization of Different Semiconductor Materials[a]

Lifetime Technique	Need for Contacts	Measured Quantity	Application for Semiconductors		
			Indirect Band Gap	Direct Band Gap	Amorphous
PC direct	Yes	Photoconductance	++	+	+++
PC-microwave	No	Reflected microwave power	+++	+	+
PC-rf bridge (resonant)	No	Eddy current (electromotive force)	++	++	+
FCA	No	Photoinduced absorption	+++	+	+
PL, (Thermography)	No	Photoemission yield	+	+++	++

[a]All the considered techniques share the common feature of using dynamic transient for lifetime extraction after pulsed excitation of excess electron hole pairs. Symbols: +, Applicable, but scarcely used; ++, relevant, commonly used; +++, beneficial, frequently used.

Table 6. Comparison between Selected Lifetime Techniques for Limiting Parameters of Measurement Conditions

Lifetime Technique	Range of injection (Δn) (cm^{-3})[a] Minimal	Maximal	Dark Conductivity Range (σ_0)[b] $(\Omega_0\,cm)^{-1}$	Measurement Bandwidth[c]	Commercial Apparatus
PC direct	10^{11}	5×10^{19}	<100	<40 THz	No information
PC-microwave	10^{9}	10^{16}	<5	<10 GHz	Yes
PC–RF bridge	10^{13}	3×10^{17}	<10	<1 GHz	Yes
FCA	10^{11}	5×10^{19}	≤200	<100 GHz	No information
PL	10^{9d}	10^{19}	≤1000	<1 THz	Yes

[a] Specified for material of low dark conductivity, $\sigma_0 = 001\ (\Omega\,cm)^{-1}$.
[b] Specified for sample thickness of 500 μm.
[c] The exact value of the bandwidth is also a function of the time duration of the utilized laser pulses. Also, detection electronics may reduce these values considerably.
[d] Depends on quantum radiation yield.

different semiconductor applications. Thus, Table 5 evaluates the advantages of each method for different types of semiconductors, while Table 6 summarizes the sensitivity and ultimate frequency range of the different methods. Notably, the frequency range indicated represents the ultimate limit of the measurement principle, while standard laboratory equipment such as photodetectors or oscilloscopes often yield a frequency limit much below 1 GHz. An exception is the PL up-conversion technique (see Fig. 21b) where pico- or femtosecond lasers may be used for characterizing ultrashort lifetimes. Finally, Table 7 summarizes some aspects of the techniques which are important for detailed recombination studies (e.g., several decades of the decay must be measured to safely extract the hl/ll-lifetime and the radiative and Auger recombination rates). Also indicated is the applicability of the techniques for lifetime mapping and for depth-resolved studies.

As a final comment, one may note that even though the principle of each method is relatively simple, some experience must be gained to evaluate aspects of, for example, surface recombination or carrier diffusion, before the derived lifetimes can be trusted as true characteristics of the semiconductor material bulk properties or as measures of the material's purity. It is, indeed, recommended that alternative methods be used to analyze the same sample. If other methods are not at one's disposal, one may gain further insight by varying the experimental conditions widely, for example, by using different injection levels, different excitation and probe areas, etc. This may hopefully unravel different recombination mechanisms and separate carrier diffusion and trapping effects from true recombination phenomena.

ACKNOWLEDGMENTS

The authors would like to acknowledge financial support from the Swedish Institute's Visby program, as well as from grant No. TAP-17/2011 of Research Council of Lithuania, from the ADOPT Linné centre and a VR project. We also thank Dr. Augustinas Galeckas for supplying the drawings (Fig. 11) to this edition.

Table 7. Comparison between Selected Lifetime Techniques for Sensitivity, hl/ll Lifetime, Depth Resolution, Mapping Resolution, and Speed

Lifetime Technique	Typical Interval of Excess Carrier Concentration in a Single Transient (Decades)[a]	hl/ll Lifetime[b]	Depth Resolution (μm)	Mapping Resolution (μm)	Data Acquisition Time for Mapping (Min)
PC direct	2–3	++	[c]	–	–
PC-microwave	2–3	+	—[c]	<100	10–30
PC–RF bridge	2–4	++	—[c]	–	–
FCA (∥)	3	++	—[c]	<10	10–30
FCA (⊥)	3–5	+++	3–5	–	–
Imaging (PL, CPL, Thermography)	1–2	—	—		1–5
PL	4–6	++	—[c]	<3	1–100

[a] The exact sensitivity is a function of the characteristics of the semiconductor material under test.
[b] Symbols: +, possible, however, causes methodical problems; ++, medium, some methodical problems; +++, easy, small methodical problems.
[c] Indirectly, through the measurements with variable absorption depth.

BIBLIOGRAPHY

"Carrier Lifetime: Free Carrier Absorption, Photoconductivity, and Photoluminescence" *in Characterization of Materials*, 1st ed., Vol. 1, pp. 427–456, by Jan Linnros, Royal Institute of Technology, Kista-Stockholm, Sweden and Vytautas Grivickas, Royal Institute of Technology, Kista-Stockholm, Sweden and Vilnius University, Vilnius, Lithuania; Published online: October 15, 2002; DOI: 10.1002/0471266965.com037.

LITERATURE CITED

Ahrenkiel, R. K. 1992. Measurement of minority-carrier lifetime by time-resolved photoluminescence. *Solid State Electron.* 35:239–250.

Ahrenkiel, R. K. and Dunlavy, D. J. 2011. A new lifetime diagnostic system for photovoltaic materials. *Solar Energy Mater. & Solar Cells.* 95:1985–1989.

Ahrenkiel, R. K. and Johnston, S. W. 2008. Lifetime analysis of silicon solar cells by microwave reflection. *Solar Energy Mater. & Solar Cells.* 92:830–835.

Ahrenkiel, R. K., Johnston, S. W., Metzger, W. K., and Dippo, P. 2007. Relationship of band-edge luminescence to recombination lifetime in silicon wafers. *J. Elect. Mat.* 37:396–402.

Ahrenkiel, R. K. and Johnston, S. W. 2003. An advanced technique for measuring minority-carrier parameters and defect properties of semiconductors. *Mat. Sci, Engin. B* 102:161–172.

ASTM. 1987. Annual Book of ASTM Standards. American Society for Testing Materials, Philadelphia.

Auston, D., Shank, C., and LeFur, P. 1975. Picosecond optical measurements of band-to-band Auger recombination of high-density plasmas in germanium. *Phys. Rev. Lett.* 35:1022–1025.

Baliga, B. J. 1987. Modern Power Devices. John Wiley & Sons, New York.

Bergman, J. P., Kordina, O., and Janzén, E. 1997. Time resolved spectroscopy of defects in SiC. *Phys. Status Solidi A* 162:65–77.

Blais, P. D. and Seiler, C. F. 1980. Measurements and retention of recombination lifetime. *In* Lifetime Factors in Silicon, ASTM STP 712, pp. 148–158. American Society for Testing and Materials, Philadelphia.

Bleichner, H., Nordlander, E., Fiedler, G., and Tove, P. A. 1986. Flying-spot scanning for the separate mapping of resistivity and minority-carrier lifetime in silicon. *Solid State Electron.* 29:779–786.

Bowden, S. and Sinton, R. A. 2007. Determining lifetime in silicon blocks and wafers with accurate expressions for carrier density. *J. Appl. Phys.* 102:124501–7.

Brandt, O., Yang, H., and Ploog, H. 1996. Images of recombination centers on the spontaneous emission of semiconductors under steady-state and transient conditions. *Phys. Rev. B* 54:R5215–R5218.

Brüggemann, R. 1997. Hole response time and the experimental test of the Einstein relation. *Phys. Rev. B.* 56:6408–6411.

Cutolo, A. 1998. Selected contactless optoelectronic measurements for electronic applications. *Rev. Sci. Instrum.* 69:1–24.

Dziewior, J. and Schmid, W. 1977. Auger coefficients for highly doped and highly excited silicon. *Appl. Phys. Lett.* 31:346–348.

Empedocles, S. A., Norris, D. J., and Bawendi, M. G. 1996. Photoluminescence spectroscopy of single CdSe nanocrystallite quantum dots, *Phys. Rev. Lett.* 77:3873–3876.

Fleming, G. R. 1986. Chemical Applications of Ultrafast Spectroscopy. Oxford University Press, New York.

Galeckas, A., Grivickas, V., Linnros, J., Bleichner, H., and Hallin, C. 1997b. Free carrier absorption and lifetime mapping in 4H SiC epilayers. *J. Appl. Phys.* 81:3522–3525.

Galeckas, A., Linnros, J., Frischholz, M., and Grivickas, V. 2001. Optical characterization of excess carrier lifetime and surface recombination in 4H/6H–SiC. *Appl. Phys. Lett.* 79:365–367.

Galeckas, A., Linnros, J., Grivickas, V., Lindefelt, U., and Hallin, C. 1997a. Auger recombination in 4H–SiC: Unusual temperature behavior. *Appl. Phys. Lett.* 71:3269–3271.

Galeckas, A., Linnros, J., and Pirouz, P. 2006. Recombination-induced stacking foults: evidence for a generation mechanism in hexagonal SiC. *Phys. Rev. Lett.* 96:025502.

Giesecke, J. A., Schubert, M. C., Michl, B. Schindler, F., and Warta, W. 2011. Minority carrier lifetime imaging of silicon wafers calibrated by quasi-steady-state photoluminescence. *Solar Energy Mater. & Solar Cells* 95:1011–1018.

Glunz, S. W. and Warta, W. 1995. High resolution lifetime mapping using modulated free carrier absorption. *J. Appl. Phys.* 77:3243–3247.

Graff, K. and Fisher, H. 1979. Carrier lifetime in silicon and its impact on solar cell characteristics. *Top. Appl. Phys.* 31:173–211.

Graff, K. and Pieper, H. 1980. Carrier lifetime measurements for process monitoring during device production. *In* Lifetime Factors in Silicon, ASTM STP 712, pp. 136–147. American Society for Testing and Materials, Philadelphia.

Grivickas, P. 2004. PhD Thesis, Optical Studies of Carrier Transport and Fundamental Absorption in 4H–SiC and Si, ISRN KTH/FTE/FR-2004/1-SE, 0284-545, Stockholm, Royal Institute of Technology.

Grivickas, P., McCluskey, M. D., and Gupta, Y. M. 2011. Order-of-magnitude reduction of carrier lifetimes in [100] *n*-type GaAs shock-compressed to 4 GPa. *Appl. Phys. Lett.* 98:092107.

Grivickas, V., Bikbajevas, V., Gulbinas, K., Gavryushin, V., and Linnros, J. 2007. Strong photoacoustic oscillations in layered $TlGaSe_2$ semiconductor. *Phys. Stat. Sol. (b)* 244: 4624–4628.

Grivickas, V., Galeckas, A., Grivickas, A., Linnros, J., and Bikbajevas, V. 2001. Excess free carrier optical excitation spectroscopy in indirect semiconductors. *Mater. Sci. (Medžiagotyra)* 7:203–208.

Grivickas, V., Linnros, J., Galeckas, A., and Bikbajevas V. 1996. Relevance of the exciton effect on ambipolar transport and Auger recombination in silicon at room temperature. *In* Proceedings of the 23rd International Conference on the Physics of Semiconductors, Vol. 1 pp. 91–94. World Scientific, Singapore.

Grivickas, V., Linnros, J., Vigelis, A., Seckus, J., and Tellefsen, J. A. 1992. A study of carrier lifetime in silicon by laser-induced absorption: A perpendicular geometry measurement. *Solid State Electron.* 35:299–310.

Grivickas, V., Galeckas, A., Bikbajevas, V., Linnros, J., and Tellefsen, J. A. 2000. Spatially and time resolved infrared absorption for optical and electrical characterization of indirect band gap semiconductors. *Thin Solid Films* 364:181–185.

Grivickas, V., Gulbinas, K., Manolis, G., Kato, M., and Linnros, J. 2010. Internal stress in freestanding 3C–SiC gown on Si and relation to carrier lifetime. *AIP Confer. Proc.* 1292:91–94.

Grivickas, V., Noreika, D., and Tellefsen, J. A., 1989. Surface and Auger recombinations in silicon wafers of high carrier density [in Russian]. *Lithuanian Phys. J.* 29:48–53; ASTM STP 712 (Sov. Phys. Collect.) 29: 591–597.

Grivickas, V. and Willander, M. 1999. Bulk lifetimes of photogenerated carriers in intrinsic c-Si. *In* EMIS Data Review no. 20, Properties of Crystalline Silicon, pp. 708–711. INSPEC, London.

Grivickas, V., Willander, M., and Vaitkus, J. 1984. The role of intercarrier scattering in excited silicon. *Solid State Electron.* 27:565–572.

Fisher, B. R., Eisler, H.-J., Stott, N. E., and Bawendi, M. G. 2004. Emission intensity dependence and single-exponential behavior in single colloidal quantum dot fluorescence lifetimes. *J. Phys. Chem. B* 108:143–148.

Häcker, R. and Hangleiter, A. 1994. Intrinsic upper limits of the carrier lifetime in silicon. *J. Appl. Phys.* 75:7570–7572.

Hall, R. N. 1952. Electron–hole recombination in germanium. *Phys. Rev.* 87:387–387.

Horanyi, T. S., Pavelka, T., and Tuttö, P. 1993. In situ bulk lifetime measurement on silicon with a chemically passivated surface. *Appl. Surf. Sci.* 63:306–311.

Ichimura, M. 2006. Temperature dependence of a slow component of excess carrier decay curves. *Solid-State Electron.* 50:1761–1766.

Itoh, A., Kimoto, T., and Matsunami, H. 1996. Exciton-related photoluminescence in 4H–SiC grown by step-controlled epitaxy. *Jpn. J. Appl. Phys.* 35:4373–4378.

Jarašiūnas, K. 2006. Characterization of advanced materials for optoelectronics by using UV lasers and four-wave mixing techniques. In: UV Solid-State Light Emitters and Detectors, NATO Science Series in Mathematics, Physics and Chemistry, Vol. 144, Kluwer Academic Publishers., pp. 93.

Jacobsen, R. H., Birkelund, K., Hoist, T., Jepsen, U. P., and Keiding, S. R., 1996. Interpretation of photocurrent correlation measurements used for ultrafast photoconductive switch characterization. *J. Appl. Phys.* 79:2649–2657.

Katayama, K., Kirino, Y., Iba, K., and Shimura, F. 1991. Effect of ultraviolet light irradiation on noncontact laser microwave lifetime measurement. *Jpn. J. Appl. Phys.* 30: L1907–L1910.

Kimoto, T., Hiyoshi, T., Hayashi, T., and Suda, J. Impacts of recombination at the surface and in the substrate on carrier lifetimes of n-type 4H–SiC epilayers. *J. Appl. Phys.* 108:083721–7.

Klein, P. B. 2008. Carrier lifetime measurement in n^- 4H–SiC epilayers. *J. Appl. Phys.* 103:003702.

Klein, P. B., Shrivarastava, A., and Sudarshan, T. S. 2011. Slow de-trapping of minority holes in n-type 4H–SiC epilayers. *Phys. Stat. Sol. (A)* 108:2790–2795.

Kull, M., Coutaz, J. L., Manneberg, G, and Grivickas, V. 1989 Absorption saturation and photodarkening in semiconductor doped glasses. *Appl. Phys. Lett.* 54:1830–1833.

Kunst, M. and Beck, G. 1988. The study of charge carrier kinetics in semiconductors by microwave conductivity measurements. II. *J. Appl. Phys.* 63:1093–1098.

Landsberg, P. T. 1987. Trap-Auger recombination in silicon of low carrier densities. *Appl. Phys. Lett.* 50:745–747.

Lee, C. H. (ed.), 1984. Picosecond Optoelectronic Devices. Academic Press, San Diego.

Ling, Z. G., Ajmera, P. K., Anselment, M., and DiMauro, L. F. 1987. Lifetime measurements in semiconductors by infrared absorption due to pulsed optical excitation. *Appl. Phys. Lett.* 51:1445–1447.

Linnros, J. 1998a. Carrier lifetime measurements using free carrier absorption transients: I. Principle and injection dependence. *J. Appl. Phys.* 84:275–283.

Linnros, J. 1998b. Carrier lifetime measurements using free carrier absorption transients: II. Lifetime mapping and effects of surface recombination. *J. Appl. Phys.* 84:284–291.

Linnros, J. and Grivickas, V. 1994. Carrier diffusion measurements in silicon with a Fourier-transient-grating method. *Phys. Rev. B* 50:16943–16955.

Linnros, J., Norlin, P., and Hallén, A. 1993. A new technique for depth resolved carrier recombination measurements applied to proton irradiated thyristors. *IEEE Trans. Electron Devices* 40:2065–2073.

Linnros, J., Lalic, N., Galeckas, A., and Grivickas, V. 1999. Analysis of the stretched exponential photoluminescence decay from nanometer-sized silicon crystals in SiO_2. *J. Appl. Phys.* 86:6128–6134.

Malinauskas, T., Jarašiūnas, K., Ivakin, E. 2010. Determination of carrier diffusion coefficient and lifetime in single crystalline CVD diamonds by light-induced transient grating technique. *Physica Status Solidi A* 207:2058–2063.

Macdonald, D. and Cuevas, A. 1999. Trapping of minority carriers in multicrystalline silicon. *Appl. Phys. Lett.* 74:1710–1712.

Macdonald, D. and Cuevas, A. 2003. Validity of simplified Shockley–Read–Hall statistics for modeling carrier lifetimes in crystalline silicon. *Phys. Rev. B.* 67:075203.

Moerner, W. E. and Fromm, D. P. 2003. Methods of single-molecule fluorescence spectroscopy and microscopy. *Rev. Sci. Instrum.* 74:3597–3619.

Orton, J. W. and Blood, P. 1990. The Electric Characterization of Semiconductors: Measurement of Minority Carrier Properties. Academic Press, London.

Otaredian, T. 1993. Separate contactless measurement of bulk lifetime and surface recombination velocity by harmonic optical generation of the excess carriers. *Solid State Electron.* 36:163–172.

Othonos, A., 1998. Probing ultrafast carrier and phonon dynamics in semiconductors. *J. Appl. Phys.* 83:1789–1830.

Pang, S. K. and Rohatgi, A. 1991. Record high recombination lifetime in oxidized magnetic Czochralski silicon. *Appl. Phys. Lett.* 59:195–197.

Pasiskevicius, V., Deringas, A., and Krotkus, A., 1993. Photocurrent nonlinearities in ultrafast optoelectronic switches. *Appl. Phys. Lett.* 63:2237–2239.

Pavesi, L. and Guzzi, M. 1994. Photoluminescence of $Al_xGa_{1-x}As$ alloys. *J. Appl. Phys.* 75:4779–4842.

Pidgeon, C. R. 1980. Free carrier optical properties of semiconductors. *In* Vol. 2 (T.S. Moss, ed.) Handbook on Semiconductors 223. North-Holland Publishing, Amsterdam, The Netherlands.

Ramspeck, K., Reissenweber, S., Schmidt, J., Bothe, K., and Brendel R. 2008. Dynamic carrier lifetime imaging of silicon wafers using an infrared-camera-based approach. *Appl. Phys. Lett.* 93:102104.

Rohatgi, A., Weber, E. R., and Kimerling, L. C. 1993. Opportunities in silicon photovoltaics and defect control in photovoltaic materials. *J. Electron. Mater.* 22:65–72.

Roman, H. E. and Pavesi, L. 1996. Monte-Carlo simulations of the recombination dynamics in porous silicon. *J. Phys. Condens. Matter* 8:5161–5176.

Ryvkin, S. M. 1964. Photoelectric Effects in Semiconductors. Consultants Bureau, New York.

Sanii, F., Giles, F. P., Schwartz, R. J., and Gray, J. L. 1992. Contactless nondestructive measurement of bulk and surface recombination using frequency-modulated free carrier absorption. *Solid State Electron.* 35: 311–317.

Ščajev, P., Usikov, A., Soukhoveev, V., Aleksiejūnas, R., and Jarašiūnas, K. 2011. Diffusion-limited nonradiative recombination at extended defects in hydride vapor phase epitaxy GaN layers. *Appl. Phys. Lett.* 98: 202105.

Schlangenotto, H., Maeder, H., and Gerlach, W. 1974. Temperature dependence of the radiative recombination coefficient in silicon. *Phys. Status Solidi A* 21:357–367.

Schlegel, G., Bohnenberger, J., Potapova, I., and Mews, A. 2002. Fluorescence decay time of single semiconductor nanocrystals. *Phys. Rev. Lett.* 88:137401–4.

Schmidt, J., Bothe, K., and Hezel, R. 2002. Oxygen-related minority- carrier trapping centers in p-type Czochralsky silicon. *Appl. Phys. Lett.* 80:4395–4397.

Schroder, D.K. 1990. Semiconductor Material and Device Characterization. John Wiley & Sons, New York.

Schroder, D. K. 1997. Carrier lifetimes in silicon. *IEEE Trans. Electron Devices* 44:160–170.

Schubert, M. C., Riepe, S. Bermejo, S. And Warta, W. 2006. Determination of spatially resolved trapping parameters in silicon with injection dependent carrier density imaging. *J. Appl. Phys.* 99:114908.

Schüler, N., Hahn, T., Schmerler, S., Hahn, S., Dornich, K., and Niklas, J.R. 2010. Simulations of photoconductivity and lifetime for steady state and nonsteady state measurements. *J. Appl. Phys.* 107:064901.

Shah, J. 1988. Ultrafast luminescence spectroscopy using sum frequency generation. *IEEE J. Quantum Electron.* 24:276–288.

Shockley, W. and Reed, W. T. 1952. Statistics of the recombination of holes and electrons. *Phys. Rev.* 87:835–843.

Sinton, R. and Cuevas, A. 1996. Contactless determination of current–voltage characteristics and minority-carrier lifetimes in semiconductors from quasi-steady-state photoconductance data. *Appl. Phys. Lett.* 69:2510–2512.

Smith, P. R., Auston, D. H., Johnson, A. M., and Augustyniak, W. M. 1981. Picosecond photoconductivity in radiation-damaged silicon-on-sapphire films. *Appl. Phys. Lett.* 38:47–50.

Sproul, A. B. 1994. Dimensionless solution of the equation describing the effect of surface recombination on carrier decay in semiconductors. *J. Appl. Phys.* 76:2851–2854.

Stachowitz, R., Schubert, M., and Fuhs, W. 1995. Nonradiative recombination and its influence on the lifetime distribution in amorphous silicon (α-Si:H). *Phys. Rev. B* 52: 10906–10914.

Strauss, U., Ruhle, W. W., and Köhler, K., 1993. Auger recombination in intrinsic GaAs. *Appl. Phys. Lett.* 62:55–57.

Swiatkowski, C., Sanders, A., Buhre, K.-D., and Kunst, M. 1995. Charge-carrier kinetics in semiconductors by microwave conductivity measurements. *J. Appl. Phys.* 78:1763–1775.

Sze, S. M. 1981. Physics of Semiconductor Devices, 2nd ed. John Wiley & Sons, New York.

Tiedje, T., Haberman, J. I., Francis, R. W., and Ghosh, A. K. 1983. An RF bridge technique for contactless measurement of the carrier lifetime in silicon wafers. *J. Appl. Phys.* 54:2499–2503.

Van Roosbroeck, W. and Shockly, W. 1954. Photon-radiative recombination of electrons and holes in germanium. *Phys. Rev.* 94:1558–1560.

Waldmeyer, J. 1988. A contactless method for determination of carrier lifetime, surface recombination velocity, and diffusion constant in semiconductors. *J. Appl. Phys.* 63:1977–1983.

Warta, W. 2006. Advanced defects and impurity diagnostics in silicon based on carrier lifetime measurements. *Phys. Stat. Sol. (a)* 203:732–746.

Wight, D. R. 1990. Electron lifetime in p-type GaAs: Hole lifetime in n-type GaAs. In EMIS Data Review No. 2, Properties of Gallium Arsenide, pp. 95, 107. INSPEC, London.

Yablonovitch, E., Allara, D. L., Chang, C. C., Gmitter, T., and Bright, T. B. 1986. Unusually low surface recombination velocity on silicon and germanium surfaces. *Phys. Rev. Lett.* 57:249–252.

Yablonovitch, E. and Gmitter, T. J. 1992. A contactless minority lifetime probe of heterostructures, surfaces, interfaces and bulk wafers. *Solid State Electron.* 35:261–267.

Yang, S. and Kelley, D. F. 2006. Transient absorption and dynamics of InSe nanoparticles. *J. Phys. Chem.* 110:13430–13435.

Zwiller, V., Pistol, M.-E., Hessman, D., Cederström, R., Seifert, W., and Samuelson, L. 1999. Time-resolved studies of single semiconductor quantum dots. *Phys. Rev. B* 59:5021–5025.

KEY REFERENCES

Ahrenkiel, 1992. See above,

Measurement theory and PL methods are described in connection with important developments in the Groups III–V material technology.

Warta, 2006. See above.

Injection- and temperature-dependent carrier lifetime spectroscopy and infrared imaging capabilities are outlined for microcrystalline Si solar cells; the role of trapping states is elucidated.

Orton and Blood, 1990. See above.

Unified account of the physical principles of electrical characterization of semiconductors related to measurement of minority carrier properties.

Klein, 2008. See above.

Describes the basis of measurement techniques and measurement conditions on measured carrier lifetime in 4H–SiC both experimentally and through detailed carrier dynamic simulations.

Jarašiūnas, 2006. See above.

Provides a comprehensive survey of transient grating measurements and characteristics of advanced materials for optoelectronics.

Schroder, 1997. See above.

A review paper where various recombination mechanisms are discussed for silicon and the concept of recombination and generation lifetime is presented.